Available online at www.sciencedirect.com

ScienceDirect

Geochimica et Cosmochimica Acta 141 (2014) 628–655

Geochimica et Cosmochimica Acta

www.elsevier.com/locate/gca

Iron and manganese speciation and cycling in glacially influenced high-latitude fjord sediments (West Spitsbergen, Svalbard): Evidence for a benthic recycling-transport mechanism

Laura M. Wehrmann [a,b,*], Michael J. Formolo [b,1], Jeremy D. Owens [a,2], Robert Raiswell [c], Timothy G. Ferdelman [b], Natascha Riedinger [a], Timothy W. Lyons [a]

[a] Department of Earth Sciences, University of California, Riverside, CA, USA
[b] Biogeochemistry Department, Max Planck Institute for Marine Microbiology, Bremen, Germany
[c] School of Earth and Environment, Leeds University, Leeds, UK

Received 16 August 2013; accepted in revised form 9 June 2014; available online 20 June 2014

Abstract

Glacial environments may provide an important but poorly constrained source of potentially bioavailable iron and manganese phases to the coastal ocean in high-latitude regions. Little is known about the fate and biogeochemical cycling of glacially derived iron and manganese in the coastal marine realm. Sediment and porewater samples were collected along transects from the fjord mouths to the tidewater glaciers at the fjord heads in Smeerenburgfjorden, Kongsfjorden, and Van Keulenfjorden along Western Svalbard. Solid-phase iron and manganese speciation, determined by sequential chemical extraction, could be linked to the compositions of the local bedrock and hydrological/weathering conditions below the local glaciers. The concentration and sulfur isotope composition of chromium reducible sulfur (CRS) in Kongs- and Van Keulenfjorden sediments largely reflect the delivery rate and isotope composition of detrital pyrite originating from adjacent glaciers. The varying input of reducible iron and manganese oxide phases and the input of organic matter of varying reactivity control the pathways of organic carbon mineralization in the sediments of the three fjords. High reducible iron and manganese oxide concentrations and elevated metal accumulation rates coupled to low input of "fresh" organic matter lead to a strong expression of dissimilatory metal oxide reduction evidenced in very high porewater iron (up to 800 μM) and manganese (up to 210 μM) concentrations in Kongsfjorden and Van Keulenfjorden. Sediment reworking by the benthic macrofauna and physical sediment resuspension via iceberg calving may be additional factors that promote extensive benthic iron and manganese cycling in these fjords. On-going benthic recycling of glacially derived dissolved iron into overlying seawater, where partial re-oxidation and deposition occurs, facilitates the transport of iron across the fjords and potentially into adjacent continental shelf waters. Such iron-dominated fjord sediments are likely to provide significant fluxes of potentially bioavailable iron to

* Corresponding author at: Department of Earth Sciences, University of California, Riverside, 900 University Ave., Riverside, CA 92521-0423, USA. Tel.: +1 (951)827 3728; fax: +1 (951)827 4324.

E-mail addresses: laura.wehrmann@ucr.edu (L.M. Wehrmann), michael-formolo@utulsa.edu (M.J. Formolo), jowens@whoi.edu (J.D. Owens), r.raiswell@see.leeds.ac.uk (R. Raiswell), tferdelm@mpi-bremen.de (T.G. Ferdelman), natascha.riedinger@ucr.edu (N. Riedinger), timothy.lyons@ucr.edu (T.W. Lyons).

[1] Present address: Upstream Research Company, ExxonMobil, Houston, TX, USA.
[2] Present address: Geology and Geophysics Department, Woods Hole Oceanographic Institution, Woods Hole, MA, USA.

http://dx.doi.org/10.1016/j.gca.2014.06.007

coastal waters and beyond. By contrast, low delivery of reducible iron (oxyhydr)oxide phases and elevated organic carbon mineralization rates driven by elevated input of "fresh" marine organic matter allow organoclastic sulfate reduction to dominate carbon remineralization at the outer Smeerenburgfjorden sites, which may limit iron fluxes to the water column.

1. INTRODUCTION

Iron plays a vital role in controlling primary production, biological carbon export, and nitrogen fixation in many parts of the ocean (e.g., Martin and Fitzwater, 1988; Coale et al., 1996; Falkowski, 1997; Hutchins and Bruland, 1998; Falkowski et al., 1998; Boyd et al., 2000). Growing awareness of the essential role of iron for primary productivity in many ocean regions and the discovery of an apparent tight linkage of changes in iron supply to the ocean with glacial-interglacial variations in atmospheric CO_2 concentrations (Martin, 1990; Jickells et al., 2005) has steered a large body of research devoted to the biogeochemical iron cycle over the past decades. Many studies have focused on the role of aeolian dust as a source of bioavailable iron to the ocean (e.g., Bruland et al., 1994; de Baar and de Jong, 2001; Jickells and Spokes, 2001; Moore and Braucher, 2008) and, more recently, on benthic iron remobilization from shelf sediments (e.g., Johnson et al., 1999; Elrod et al., 2004; Moore and Braucher, 2008; Severmann et al., 2010; Noffke et al., 2012; Homoky et al., 2013). Iron deriving from glacial environments represents the least constrained source of iron to the ocean (Raiswell et al., 2006). There is growing awareness that glacial environments may provide this key nutrient to high latitude ocean regions, where this source likely dominates over other iron fluxes to coastal waters (Statham et al., 2008; Raiswell et al., 2008a; Lippiatt et al., 2010; de Jong et al., 2012; Wadham et al., 2010; Wadham et al., 2013; Gerringa et al., 2012; Bhatia et al., 2013; Hawkings et al., 2014).

Glacial environments have been identified as important microbial habitats (Sharp et al., 1999; Skidmore et al., 2000; Gaidos et al., 2004; Mikucki et al., 2004; Lanoil et al., 2009) that function as crucial sites for the transformation of different carbon pools and for the microbially enhanced chemical weathering of glacial debris on the surface, below, and within ice sheets and glaciers (e.g., Tranter et al., 2003; Wadham et al., 2004; Skidmore et al., 2005; Wadham et al., 2010; Montross et al., 2012; Stibal et al., 2012). Biogeochemical weathering processes in subglacial and proglacial environments include (1) oxidation of sulfide minerals by oxygen, Fe(III), and nitrate; (2) dissolution of carbonates; and (3) silicate weathering (see Tranter et al., 2003; Skidmore et al., 2010; Wadham et al., 2013; for review). These weathering processes yield, for example, sulfate, bicarbonate, magnesium, calcium ions, and nutrients such as iron and phosphorus to glacial runoff waters (Wadham et al., 2001; Cooper et al., 2002; Tranter, 2005). Oxic glacial runoff may provide a comparably small amount of dissolved iron to coastal waters (Statham et al., 2008; Raiswell and Canfield, 2012; Wadham et al., 2013) that is accompanied by a large fraction of iron (oxyhydr)oxides and other, mechanically weathered, particulate iron phases (Poulton and Raiswell, 2002, 2005; Raiswell et al., 2006). In contrast, anoxic runoff waters, entering coastal waters below tidewater glaciers, ice-sheets, and by groundwater discharge, may provide additional iron sources with higher aqueous and colloidal/nanoparticulate iron components (Skidmore et al., 2010; Raiswell and Canfield, 2012; Wadham et al., 2013). Icebergs and sea-ice contain nanoparticulate iron(oxyhydr)oxides preserved in the frozen matrix that can evade deposition in fjord sediments and thus reach open ocean waters (e.g., Raiswell et al., 2006, 2008a,b, 2009; Lannuzel et al., 2010; van der Merwe et al., 2011; de Jong et al., 2013). Accordingly, these ice-borne inputs are now regarded as important sources of bioavailable iron to high-nutrient, low-chlorophyll areas of the Southern Ocean and Antarctic (Raiswell et al., 2006; Smith et al., 2007; Lannuzel et al., 2007, 2008; Raiswell et al., 2008a; Lin et al., 2011; Shaw et al., 2011).

Glacially derived iron enters adjacent ocean waters in aqueous (here defined as <0.02 μm) plus colloidal/nanoparticulate (collectively termed 'dissolved iron') and particulate forms (>1 μm; Raiswell et al., 2006; Raiswell and Canfield, 2012). The composition and physico-chemical reactions of the iron pool determine its bioavailability and thus ultimately the potential to fuel primary production in surface waters (Moore and Braucher, 2008; Tagliabue et al., 2009; Breitbarth et al., 2010). Aqueous, colloidal, and nanoparticulate iron phases exhibit varying degrees of bioavailability (Hutchins et al., 1999; Yoshida et al., 2002; Kraemer, 2004; Borer et al., 2005; Shaked et al., 2005; Hunter and Boyd, 2007; Boyd and Ellwood, 2010; Breitbarth et al., 2010; Raiswell and Canfield, 2012; Shaked and Lis, 2012). Aqueous iron, which mainly occurs as Fe(III) bound to organic ligands in marine seawater (van den Berg, 1995; Rue and Bruland, 1995; Hassler et al., 2011), is suggested to be bioavailable, although the ligand type may determine its availability for specific groups of organisms (see Hunter and Boyd, 2007, and Gledhill and Buck, 2012, for review). Colloidal/nanoparticulate species, which are suggested to be composed of small iron (oxyhydr)oxide and organic matter subunits (Boyé et al., 2010; Raiswell and Canfield, 2012), are believed to be only partially bioavailable to eukaryotic organisms (Chen and Wang, 2001; Chen et al., 2003; Cullen et al., 2006).

Manganese also functions as a micronutrient (Sunda et al., 1981; Coale, 1991; Morel and Price, 2003), and the scavenging of trace metals by manganese oxides can exert a strong control on the distribution of biologically essential trace elements, such as cobalt, in continental margin environments (Knauer et al., 1982; Shaw et al., 1990). Input from continental erosion represents a main source of

manganese oxides to continental shelf waters. Here, the benthic recycling of manganese oxides and subsequent flux of manganese from the seabed represents an important pathway for the reintroduction of dissolved manganese into the water column (Heggie et al., 1987; Johnson et al., 1992; Aller, 1994; Pakhomova et al., 2007; McManus et al., 2012). The diagenetic recycling and transport of manganese from Arctic shelf sediments has been invoked as a main driver for the formation of distinct Mn-rich brown layers in adjacent slope and basin sedimentary sequences (März et al., 2011, 2012; Macdonald and Gobeil, 2012). These studies suggest that a large fraction of manganese reaching the inner Arctic shelves (<100 m water depth) must be recycled and transported to the Central Arctic Ocean in order to balance the modern manganese budget of the Arctic.

Given the large volume of glacial runoff in many high-latitude regions, adjacent fjords represent important depocenters for glacially derived iron and manganese. However, little is known about the cycling and transfer of these metals in the fjords, which ultimately represent the transition between the glacial and marine environments. A large fraction of aqueous and nanoparticulate iron phases originating from glacial sources is suggested to precipitate during their passage across the salinity gradient from glaciers to adjacent coastal waters (e.g., Lippiatt et al., 2010), for example, as iron (oxyhydr)oxide coatings on particles. Glacial runoff waters, however, generally also contain a large fraction of particulate iron phases, with concentrations exceeding those of dissolved iron by orders of magnitude (Poulton and Raiswell, 2005; Raiswell et al., 2006; Lippiatt et al., 2010). The fate of the large amounts of iron (oxyhydr)oxides delivered to fjords directly by glacial runoff, or indirectly through precipitation of dissolved glacial iron, remains poorly understood. It is assumed that further coagulation in saline fjord waters results in trapping of 90% of these iron phases in fjord sediments (Raiswell, 2006; Raiswell et al., 2006). Biogeochemical processes in these fjords, particularly in the fjord sediments, have not been considered previously, but these processes may strongly affect the distribution and speciation of iron phases and ultimately alter the bioavailability of the glacially derived iron phases.

A better understanding of the input of glacially derived iron and manganese, and the processes and feedbacks that tie the iron cycle to recent climate change, are needed for the Arctic environment. The Arctic Ocean is very susceptible to global climate change through various feedback mechanisms (Anisimov et al., 2007; Meehl et al., 2007; Spielhagen et al., 2011). For instance, sea-ice cover of the Arctic Ocean is retreating unexpectedly fast (Shimada et al., 2006; Comiso et al., 2008; Giles et al., 2008; Perovich et al., 2008), thus exposing increasingly large areas of this region to sunlight. This change may allow for enhanced phytoplankton growth in summer (Arrigo et al., 2008; Slagstad et al., 2011), depending on the availability of nutrients to sustain summer primary production (Carmack et al., 2006; Popova et al., 2010). The input of iron may become one limiting factor for primary productivity, especially if ice-borne transport of iron to the open ocean is reduced in a warming climate (Carmack et al., 2006). Runoff from local glaciers may provide additional input of dissolved and colloidal iron to coastal waters and potentially beyond (Statham et al., 2008; Lippiatt et al., 2010; Gerringa et al., 2012). Shelf areas of the Arctic are at present responsible for a disproportionately high fraction of primary production of up to 24% (Pabi et al., 2008; Popova et al., 2010), and the southeast Greenland Sea and the Barents Sea around Svalbard are amongst the most productive areas of the Arctic Ocean (Sakshaug, 2004; Carmack et al., 2006; Popova et al., 2010). The glaciers of the Svalbard Archipelago have retreated significantly in the past 50 years (Dowdeswell, 1995; Nordli et al., 1996; Ziaja, 2001; Kohler et al., 2007), and there is evidence for unprecedented increases in summer temperatures compared to the past 1800 years in this region (Spielhagen et al., 2011; D'Andrea et al., 2012). The Svalbard fjords thus represent excellent model locations to evaluate the coupling between climatic changes, glacial iron delivery mechanisms, and biogeochemical feedback processes.

In this study, we take a comprehensive approach in our examination of the biogeochemical processes in fjord sediments of three Western Svalbard fjords: Smeerenburgfjorden, Kongsfjorden, and Van Keulenfjorden. First, we determine how the local bedrock geology and the glacial coverage may affect the speciation and amount of delivered iron and manganese, water column productivity, and quality of deposited organic matter. The three chosen fjords are very different with respect to their bedrock composition and the size of the catchment area glacial coverage. We hypothesize that glaciated areas characterized by relatively Fe-poor lithologies deliver glacial flour low in reducible iron to the adjacent fjords. In contrast, iron- and pyrite-rich rock types, such as sandstones, may allow for the mechanical and biogeochemical production of higher amounts of dissolved iron and iron (oxyhydr)oxide phases compared to igneous and metamorphic bedrock lithologies. Second, the extent of glacial coverage in the fjord-surrounding areas may affect the volume and suspended load of glacial runoff and thus ultimately the amount of weathered iron and manganese phases that are delivered to the adjacent fjords. Third, we tie these findings to the prevailing sedimentary biogeochemical processes and elucidate the resulting differences amongst the different fjords. We specifically investigate how the biogeochemical processes control the fixation, remobilization, and ultimately the down-fjord transport of glacially derived iron and manganese phases. We shed light on the diagenetic cycling of these phases as an additional, previously unconsidered, mechanism that may aid the transfer of glacially derived metals across fjords to the outer shelf. Finally, we discuss the biogeochemical processes in the glacially influenced fjords within the context of the sensitivity of the Arctic region to recent climate change.

2. STUDY AREA

Spitsbergen is the largest island of the Svalbard Archipelago, located between 74° and 81° N in the high Arctic (Fig. 1). Polythermal and cold-based glaciers with thicknesses of more than 100 m cover ~36,600 km^2 of Svalbard

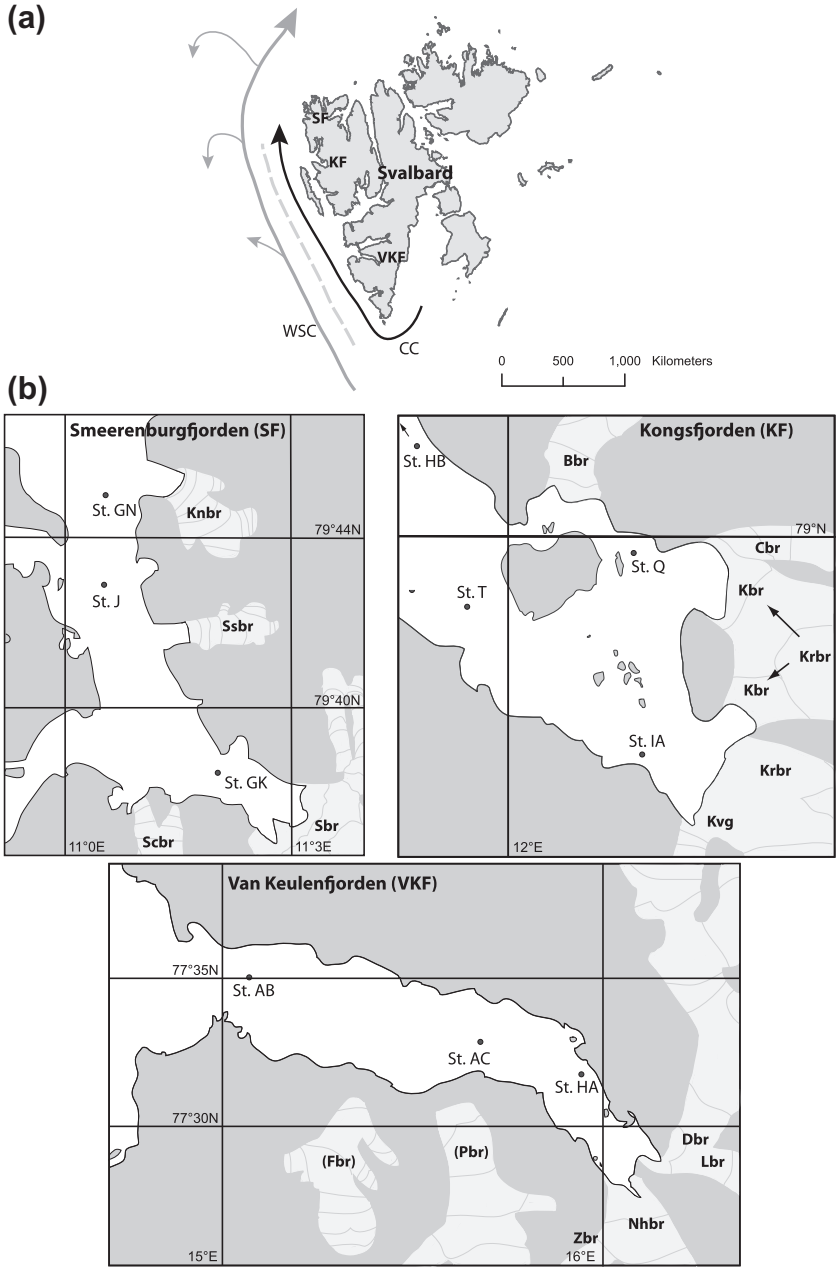

Fig. 1. (a) Map of the Svalbard archipelago including locations of Smeerenburgfjorden (SF), Kongsfjorden (KF) and Van Keulenfjorden (VKF). Light grey and black arrows indicate the flow paths of the Western Spitsbergen Current (WSC) and the Coastal Current (CC), and the dashed line denotes the location of the Western Spitsbergen Arctic Front (after Saloranta and Svendsen, 2001). (b) Detailed maps of Smeerenburgfjorden including sampling Stations GK, J and GN, Kongsfjorden including sampling Stations Q, IA, T, and HB, and Van Keulenfjorden including sampling Stations HA, AC, and AB. Light grey areas indicate the locations of large glaciers (>6 km^2). In Smeerenburgfjorden these are Smeerenburgbreen (Sbr), Scheibreen (Scbr), Kennedybreen (Knbr) and Sellstrømbreen (Ssbr). Kongsfjorden hosts Blomstrandbreen (Bbr), Conwaybreen (Cbr), Kongsvegen (Kvg), and Kronebreen (Krbr) which partially leads into Kongsbreen (Kbr). In Van Keulenfjorden, Zwadzkibreen (Zbr), Nathorstbreen (Nhbr), Liestølbreen (Lbr), and Doktorbreen (Dbr) are located, as well as the land-terminating large glaciers Finsterwalderbreen (Fbr) and Penckbreen (Pbr). Note that smaller glaciers are not marked on the maps.

(Hagen et al., 1993). The majority of the glaciers terminate in the sea with calving ice-cliffs. They are often surging-type glaciers. The Svalbard glaciers are commonly characterized by extensive subglacial drainage systems delivering large amounts of suspended material directly into the adjacent fjord waters (e.g., Hagen et al., 1993; Hodgkins, 1997; Hodgkins et al., 2003; Rippin et al., 2003). In addition, the fjord systems are influenced by glacial runoff from non-sea-terminating glaciers crossing vast proglacial plains (Wadham et al., 2007; Hodgkins et al., 2009). The three

investigated fjords—Smeerenburgfjorden, Kongsfjorden, and Van Keulenfjorden—are located on the western side of Spitsbergen (Fig. 1).

All three fjords host large tidewater glaciers at the fjord heads and several smaller glaciers, which enter the fjords along the shores or deliver runoff by glacial streams (Fig. 1b). The glacier sizes and the total glacial coverage at Smeerenburgfjorden are, however, small compared to glacier sizes and coverage in Kongsfjorden and Van Keulenfjorden areas (Table 1). Due to multiple periods of glacier advance and retreat, the fjords are separated by large ridges into several basins that reach water depths of >350 m (Howe et al., 2003; Ottesen et al., 2008). Sediment coverage within the fjords is >30 m in the innermost basins but decreases seaward (Howe et al., 2003; Velle, 2012). Sedimentation rates in the three fjords can reach values of up to 30,000 cm $kyrs^{-1}$ and generally decrease downfjord. These rates are suggested to be highly variable depending on glacial activity in the respective catchment area (e.g., Kempf et al., 2013).

The catchment area bedrock compositions of the three fjords are very different (Table 1). At Smeerenburgfjorden, the bedrock comprises metamorphosed basement with granite, migmatite, and banded gneiss of the Mesoproterozoic Caledonian Smeerenburgfjorden Complex in the northern and southwestern parts. The southeastern and southern Smeerenburgfjorden bedrock is characterized by the intrusive Hornemantoppen Granite (Silurian-Devonian boundary; Dallmann et al., 2002; Ohta et al., 2007; Ohta et al., 2008). These type of bedrock lithologies have total iron concentrations generally averaging around 2 wt.% (Taylor, 1964) and are relatively low in pyrite (e.g., Blatt et al., 2005). The geology of the North Kongsfjorden area is characterized by mid-Proterozoic metamorphosed basement rocks including phyllite, schist, marble, and bands of dolostone (Hjelle, 1993; Svendsen et al., 2002). Bedrock in the eastern Kongsfjorden area, including the catchment areas of Kronebreen and Kongsvegen, consists of Devonian sandstone, conglomerate, marble, and Carboniferous-Permian red sandstone, shale, and localized coal, and Proterozoic phyllites, schists, and carbonates (Hjelle, 1993). On the southern side of Kongsfjorden, particularly on Brøgger Peninsula, sedimentary rocks of late Paleozoic age consisting of conglomerates, sandstones, carbonates, and spiculitic rocks dominate (Hjelle, 1993). Locally, Tertiary rocks with conglomerates, sandstones, shales, and coal seams are also present (Hjelle, 1993). At the fjord mouth of Van Keulenfjorden, shale, siltstone, sandstone, dolomite, red conglomerate, and chert of Late Paleozoic to Mesozoic age are exposed along a NW-SE trend, including into the Finsterwalderbreen catchment area (Dallmann et al., 1990; Harland, 1997). In approximately mid-fjord locations, arkosic to lithic arenites of the Paleocene/Eocene Van Mijenfjorden Group are situated on both sites of the fjord (Dallmann et al., 1990; Harland, 1997). These sandstones typically have an average iron content of 3.5 wt.% (Ronov, 1982) and may contain high pyrite concentrations.

The Western Spitsbergen fjords are influenced by Atlantic Water (AW) from the Western Spitsbergen Current (WSC), which flows pole-ward along the continental slope

Table 1
Background information on the three investigated fjords including length and width, sizes of local glaciers (Blaszczyk et al., 2009), glacial coverage (Hagen et al., 1993; Svendsen et al., 2002), and bedrock composition.

Fjord	Orientation	Length [km]	Width [km]	Glaciers	Total glacial catchment area and % glacial coverage	Bedrock composition
Smeerenburgfjorden	N-S, NNW-SSE	20	5	Smeerenburgbreen (95 km^2),Scheibreen (8 km^2), Sellstrømbreen (8 km^2), Kennedybreen (6 km^2); other glaciers <6 km^2	232 km^2 (57%)	Granite, migmatite, banded gneiss
Kongsfjorden	E-W	22	12	Kronebreen (709 km^2), Kongsvegen (154 km^2), Blomstandbreen (66 km^2), Conwaybreen (35 km^2)	1100 km^2 (77%)	Sandstone, conglomerate, marble, shale, coal, phyllites, schists, carbonates
Van Keulenfjorden	E-W	40	7.5	Nathorstbreen (319 km^2), Doktorbreen (95 km^2), Liestølbreen (99 km^2), Zwadzkibreen (83 km^2)	1273 km^2 (83%)	Shale, siltstone, sandstone, dolomite, red conglomerate, chert, arkostic and lithic arenites

and western Svalbard shelf, and as the Svalbard Branch (SV) along the northern Svalbard slope (Manley, 1995; Cottier et al., 2005; Ślubowska-Woldengen et al., 2007). The AW influence is responsible for essentially ice-free conditions west of the Svalbard shelf and the delivery of large amounts of nutrients by deep convection (Popova et al., 2010). This region is thus highly productive and less influenced by inter-annual variability compared to seasonally ice-covered areas around Svalbard, e.g., to the northeast (Reigstad et al., 2011). The Svalbard shelf receives an important contribution of freshwater input from glaciers and rivers (Meredith et al., 2001; Nilsen et al., 2008). Western Spitsbergen fjords are characterized by a pronounced three-layer stratification consisting of (1) a low salinity, warm surface layer deriving from glacial meltwater and river water runoff; (2) an intermediate layer with a AW component; and (3) a cold, high salinity bottom layer (Cottier et al., 2005, 2010; Nilsen et al., 2008). This regime is most pronounced in summer and transitions to haline circulation in winter when other water masses, formed within the fjords, dominate the water column (Nilsen et al., 2008; Cottier et al., 2010). The density stratification during summer impacts the distribution of suspended particulates in the water column (Svendsen et al., 2002; Zajaczkowksi, 2008; Trusel et al., 2010). Typically, a brackish overflow layer, characterized by a high load of suspended particulate matter, develops adjacent to fjord glaciers (Trusel et al., 2010) or rises as a positively buoyant plume into the fjord waters, where meltwater emerges from a submerged glacier base (Powell, 1990; Cowan and Powell, 1991; Mugford and Dowdeswell, 2011). The discharge plume spreads laterally towards the central fjord as a radial surface gravity current, and suspended particles settle as a function of their size and due to flocculation (Kranck, 1973; Syvitski et al., 1985; Syvitski and Lewis, 1992; Mugford and Dowdeswell, 2011).

3. METHODS

3.1. Sample collection

We collected samples during two sampling campaigns in the summer months of 2010 and 2011 aboard RV *Farm*. In each fjord, stations in the innermost area, mid-fjord, and in the outermost basin were sampled (Fig. 1b). A list of the sampling locations and water depths is given in Table 2. Sediment cores were retrieved with a predrilled Rumohr gravity corer (Ø100 mm, 150–250 cm length; Meischner and Rumohr, 1974) or a Haps corer (Ø127 mm, 31.5 cm length; stations GK, T; Kanneworff and Nicolaisen, 1983). Porewater (3–4 mL) was isolated within a few hours after core retrieval by Rhizon sampling (Seeberg-Elverfeldt et al., 2005; Dickens et al., 2007) with attached syringes, and samples were preserved with zinc acetate (2%, w/v) for sulfate and sulfide concentration measurements and nitric acid (2%, v/v) for trace metal analyses. Sediment samples were collected with cut-off syringes, which were sealed headspace-free and immediately frozen. The sampling resolution for porewater and solid-phase samples was 2 cm in the top 20 cm and 4–8 cm in deeper core sections.

3.2. Solid-phase analyses

3.2.1. Iron and manganese speciation and concentrations

A sequential extraction procedure modified from Poulton and Canfield (2005) was applied to frozen 2011 samples. This extraction procedure is designed for quantification of iron and manganese bound in carbonates (1 M sodium acetate buffered with acetic acid to pH 4.5; 48 h), reducible iron and manganese oxide phases (50 g L^{-1} sodium dithionite buffered to pH 4.8 with acetic acid and sodium citrate; 2 h), and magnetite (Fe_{mag}; 0.2 M ammonium oxalate/0.17 M oxalic acid buffered with ammonium hydroxide to pH 3.2; 6 h; Poulton and Canfield, 2005). Frozen samples (0.3–0.5 g) were transferred into extraction vials, 10 mL of the respective reagent was added immediately, and N_2 was added to the vial headspace. Extractions were done at room-temperature by continuous shaking, and aliquots were taken after centrifugation (5000 rpm, 5 min). All solutions were freshly prepared prior to extraction, and reagent blanks were taken. Iron concentrations of reagent blanks were below detection limit. The sodium acetate and dithionite iron fractions are here collectively referred to as 'reducible iron' (Fe_{ox}) and encompass iron carbonates, ferrihydrite, goethite, and hematite. The reproducibility of this extraction method, checked by repeated extractions, is better than 8%, which is similar to previous studies (e.g., Poulton and Canfield, 2005; März et al., 2012). Extractable manganese (Mn_{extr}) concentrations are presented as the sum of the concentrations of adsorbed manganese (1 M $MgCl_2$, 2 h; Poulton and Canfield, 2005), Mn-carbonates, and Mn-oxides extracted by the sequential extraction. All extracts were analyzed by inductively coupled plasma-mass spectrometry (ICP-MS; Agilent 7500ce) after dilution in trace-metal grade 2% HNO_3. Total solid-phase iron (Fe_T) and aluminum (Al) concentrations were determined on ashed samples (550 °C) using a three-step digestion method (HNO_3-HF, Aqua Regia, and 6N HCl with H_2O_2). Final digest concentrations were determined on an Agilent 7500ce ICP-MS after 200-fold dilution in trace-metal grade 2% HNO_3. Precision (1σ) and accuracy of the digestion method and ICP-MS runs were monitored using United States Geological Survey (USGS) reference standards SDO-1 (Devonian Ohio Shale) and SCO-1 (Cody Shale) and were <4% and <7%, respectively. All solid-phase iron data are presented in Supplementary Table S1.

Concentrations of acid volatile sulfide (AVS) and chromium reducible sulfur (CRS) were determined on frozen sediment samples from 2011 by a two-step distillation method with cold 2 M HCl followed by a boiling 0.5 M $CrCl_2$ solution (Fossing and Jørgensen, 1989). Concentrations of sulfide released during both distillation steps and trapped in zinc acetate were measured spectrophotometrically according to Cline (1969). The amounts of iron bound as AVS and CRS were calculated from AVS and CRS sulfur concentrations using FeS and FeS_2 stoichiometries, respectively. The total amount of highly reactive iron (Fe_{HR}) is defined as $Fe_{HR} = Fe_{ox} + Fe_{mag} + Fe_{AVS} + Fe_{CRS}$. It is also presented as the fraction of the total iron pool: Fe_{HR}/Fe_T (e.g., Raiswell and Canfield, 1998).

Table 2
Sampling location and water depth of the stations sampled in Smeerenburgfjorden, Kongsfjorden and Van Keulenfjorden.

Fjord	Station	Location		Water depth [m]
Smeerenburgfjorden	GK	79°38.49N	11°20.96E	178
	J	79°42.83N	11°05.10E	214
	GN	79°45.01N	11°05.99E	198
Kongsfjorden	Q	78°54.43N	12°17.87E	48
	IA	78°53.75N	12°20.22E	57
	T	78°58.06N	11°52.91E	330
	HB	79°02.07N	11°42.12E	170
Van Keulenfjorden	HA	77°32.04N	15°50.26E	28
	AC	77°33.16N	15°39.24E	66
	AB	77°35.17N	15°04.60E	101

Iron accumulation rates, A_{Fe} [g cm^{-2} kyr^{-1}], were calculated according to Lyle and Dymond (1976) as:

$$A_{Fe} = [C_{Fe} \cdot \omega \cdot \rho \cdot (1 - X_W)] \cdot 1000 \quad (1)$$

where C_{Fe} is the average concentration of total iron in the sediment [wt.% dry weight], ω is the sedimentation rate [cm yr^{-1}], ρ is the average wet bulk density [g cm^{-3}], and X_W is the average weight fraction of water in the sediment. Sedimentation rates, wet bulk density, and water content for Smeerenburgfjorden stations were previously published in Hubert et al. (2009) and Velle (2012). Similar data from Van Keulenfjorden data are provided in Kempf et al. (2013). Calculations of iron accumulation rates for Kongsfjorden stations are based on sediment accumulation rates from Svendsen et al. (2002). Stations investigated in these previous studies are in the immediate vicinity, or at the same coring locations, as cores taken for our study.

3.2.2. Solid-phase total inorganic and organic carbon (TIC, TOC) concentrations

Sedimentary total carbon (TC) and total nitrogen (TN) contents were determined with a Carlo Erba NA-1500 CNS analyzer for dried sediment samples collected in 2010. The cores from Station T and IA (2011 samples) were analyzed with an Eltra CS analyzer. Total inorganic carbon (TIC) was analyzed using a CM 5012 CO_2 coulometer (UIC) or an Eltra CS analyzer after acidification. The total organic carbon (TOC) content was calculated as the difference between TC and TIC. The total carbon to nitrogen (C/N) ratio is presented in (mol/mol).

3.3. Stable sulfur isotope analyses of solid-phase iron sulfides

ZnS precipitates from the AVS and CRS distillations were converted to Ag_2S by treatment with $AgNO_3$ and subsequent washing with NH_4OH to remove colloidal silver. Sulfur isotope ratios were determined by weighing 0.2–0.4 mg of Ag_2S with V_2O_5 into a tin capsule followed by combustion at 1060 °C in an elemental analyzer (EURO or Costec Elemental Analyzer). Evolved SO_2 was carried by a helium stream through a gas chromatography (GC) column, a Finnigan Conflo III, and into a Finnigan Delta V stable isotope ratio mass spectrometer (Thermo Scientific). The sulfur isotope measurements were calibrated with reference materials NBS 127 ($\delta^{34}S = +20.3‰$) and IAEA-SO-6 ($\delta^{34}S = -34.1‰$). The standard error (1σ) of the measurement was less than 0.2‰ for $\delta^{34}S$. Sulfur isotope composition is reported with respect to Vienna Canyon Diablo Troilite (V-CDT).

3.4. Porewater analyses and modeling of porewater iron and manganese profiles

3.4.1. Porewater analyses

Sulfate concentrations on 10-fold diluted, zinc acetate-treated porewater samples were determined by suppressed ion chromatography (IC) using a Metrohm 761 Compact IC system (Metrohm A Supp 5 column; 3.2 mM Na_2CO_3 and 1 mM $NaHCO_3$ eluent; 20 µl sample loop) with CO_2 suppression and online removal of zinc (Metrohm A PPC 1 HC matrix elimination column). Standards were prepared from a Merck certified sulfate standard solution (1001 ± 2 mg SO_4^{2-} l^{-1}) with IAPSO seawater as a secondary reference standard. Total dissolved sulfide concentrations were measured according to Cline (1969) on the same samples (detection limit of 2 µM). This method determines the concentration of sulfur in the –II oxidation state in all sulfide species in solution, including the sulfide component of polysulfide species (Kamyshny Jr. and Ferdelman, 2010). Porewater total iron and manganese concentrations were analyzed by ICP-MS (Agilent 7500ce) on 20-fold diluted samples (2% HNO_3) with an external analytical precision (1σ) of <5%. Calibration standards where prepared with the addition of NaCl in 2% HNO_3 to match the porewater sample matrix. Drift standards, prepared the same way, were run repeatedly to evaluate instrumental drift. The method detection limit of the ICP-MS method was ~0.8 µM for Fe and ~0.5 µM for Mn. The Rhizon samplers have a mean pore size of 0.1 µm and thus generally allow for the collection of aqueous and certain nanoparticulate iron phases, which dissolve upon nitric acid treatment. Nonetheless, in reduced sediments, such as the Svalbard fjord sediments, this porewater iron consists primarily of truly reduced aqueous iron phases such as Fe^{2+} (Millero et al., 1995; Raiswell and Canfield, 2012). Importantly, the numerical modeling procedures used in the following sections are only applicable to aqueous iron, and we assume here that our porewater data correspond to this iron fraction.

3.4.2. Numerical modeling procedure

The Rate Estimation from Concentrations (REC) model (Lettmann et al., 2012) was used to calculate consumption and production rates for aqueous iron and manganese

and their fluxes toward the oxygenated surface sediment. This numerical model yields element consumption and production rates from element concentration profiles taking into account sediment tortuosity, bioturbation, and bioirrigation—similar to other common procedures (e.g., Berg et al., 1998; Wang et al., 2008). However, the REC model also applies a smoothing parameter, λ, based on a Tikhonov regularization, which simulates smooth solute concentration profiles and thus compensates for potential measurement uncertainties (Lettmann et al., 2012). Bioirrigation was neglected in our REC model, since this process is unlikely to be important at the inner fjord stations due to the high sediment accumulation rates. For example, subsurface deposit feeders only constitute 4% of infaunal macrobenthos in the inner Kongsfjorden area, while they account for almost 40% of macrobenthos in the outer fjord (Hop et al., 2002). Nevertheless, this process may further enhance the transport of iron and manganese to the water column at the outer fjord stations (Raiswell and Canfield, 2012); thus, our flux estimates likely represent minimum values. An average porosity, φ, of 0.81 was used in the model based on previous porosity measurements for Svalbard fjord sediments (e.g., Kostka et al., 1999). The effective molecular diffusion coefficient, D_E, was determined by assuming a constant diffusion coefficient in free solution for seawater at 0 °C of 3.15×10^{-10} m^2 s^{-1} for Fe^{2+} and 3.02×10^{-10} m^2 s^{-1} for Mn^{2+} (Schulz, 2006) and correcting for tortuosity, f, calculated according to Boudreau (1997) as:

$$f = 1 - \ln(\varphi^2) \quad (2)$$

Given the importance of bioturbation in Svalbard sediments (Jørgensen et al., 2005; Hubert et al., 2009), a constant bioturbation coefficient, D_B, was applied for the top 10 cm at each station, depending on the specific water depth, according to Middelburg et al. (1997):

$$D_B = 5.2 \cdot 10^{(0.7624 - 0.0003972 \cdot \text{water depth})} \quad (3)$$

Several Tikhonov parameters were tested to fit the measured iron and manganese concentration profiles for each station.

We also took into consideration iron precipitation in the oxygenated zone and estimated the flux of iron across the oxygenated surface sediment layer—that is, the amount of iron that is ultimately reaching the water column—by using the approach by Raiswell and Anderson (2005) and Homoky et al. (2012). The flux (mol cm^2 s^{-1}) of aqueous iron across the sediment–water interface, J, was calculated according to Raiswell and Anderson (2005; based on the equation by Boudreau and Scott, 1978):

$$J(Fe_{diss}) = (\varphi \cdot (D_s \cdot k_1)^{0.5} \cdot C_p) / \left(\sinh \left[\left(\frac{k_1}{D_s} \right)^{0.5} \cdot L \right] \right), \quad (4)$$

where D_s is the overall diffusion coefficient (cm^2 s^{-1}), k_1 is the first order rate constant for Fe^{2+} oxidation (s^{-1}), C_p is the porewater iron concentration (g cm^{-3}) at the bottom of the oxygenated sediment surface layer, and L is the thickness (cm) of this layer. To be consistent with the input parameters of the REC model, we used an average porosity of 0.81 and the same D_E as was used above and included D_B as a factor influencing the overall diffusion coefficient following Lettmann et al. (2012) as:

$$D_s = D_E + D_B \quad (5)$$

The output data of the REC model were used to calculate C_p. The oxygenated zone in Svalbard sediments has a thickness of 0.35 to 0.8 cm (Jørgensen et al., 2005); thus, a conservative value of 0.8 cm was used for our calculation. To derive k_1, which is a function of bottom-water oxygen concentration, we used the following (based, e.g., on Millero et al., 1987; Raiswell and Anderson, 2005):

$$k_1 = k[O_2][OH^-]^2 \quad (6)$$

assuming the bottom-water oxygen concentration of 347 μM previously determined for southwestern Svalbard fjords (Jørgensen et al., 2005), a pK_W of 14.3 at 0 °C (Millero, 2001), and a pH of 7.5 (Homoky et al., 2012). The bottom-water oxygen value reported by Jørgensen et al. (2005) is typical for high-latitude fjords, which, in contrast to temperate fjords, have continuous oxygen-rich bottom water conditions sustained by autumn turnover of the water column and low organic carbon mineralization rates (Syvitski et al. 1987; Weslawski et al., 2011). We note that a higher value for the pH would lead to lower calculated values for the dissolved iron across the sediment–water interface (Raiswell and Anderson, 2005). For example, at a pH of 7.8, calculated flux values would be up to 75% smaller than values calculated using a pH of 7.5. Oxic respiration and metal oxidation (via oxygen and/or nitrate) at the sediment–water interface, however, leads to a drop in pH (Soetaert et al., 2007) as, for example, is observed in San Clemente basin sediments by Reimers et al. (1996) and modeled by Van Cappellen and Wang (1996). A pH of 7.5 thus likely reflects the *in situ* conditions at the Svalbard stations. The variable k was based on the empirically derived relationship (Millero et al., 1987):

$$\log k = 21.56 - 1545/T - 3.29I^{0.5} + 1.52I \quad (7)$$

where I is the ionic strength of 0.723 for seawater (Raiswell and Anderson, 2005). Manganese(II) oxidation with O_2 in natural water is several orders of magnitude slower than iron(II) oxidation (see Von Langen et al., 1997; Morgan, 2005; for review), which favors the release of manganese into the overlying water column compared to aqueous iron. Additionally, the first-order rate constant for manganese oxidation is more than two orders of magnitude smaller than those for manganese adsorption and desorption (Richard et al., 2013). We therefore assume manganese oxidation to have a negligible effect on the upward porewater manganese flux and did not calculate it.

4. RESULTS

4.1. Solid-phase geochemical composition

The solid-phase iron data reveals distinct differences in the quantity of specific iron phases amongst the three fjords. The concentrations of Fe_{ox} are lowest in Smeerenburgfjorden (mostly < 0.5 wt.%) and highest in Van

Keulenfjorden sediments (< 1.2 wt.%; Fig. 2a–c). Additionally, at the Van Keulenfjorden sites, pronounced decreases are observed in Fe_{ox} concentration in the top 10 to 20 cm. Fe_{HR} concentrations, which also include the magnetite fraction and iron phases that are present as AVS and CRS, mirror these general trends (Fig. 2a–c). Pronounced increases in sedimentary AVS and CRS concentrations with depth are observed at the mid- and outer Smeerenburgfjorden stations (Fig. 2a). In contrast, AVS and CRS concentrations in Kongsfjorden and Van Keulenfjorden sediment show only subtle increases and remain at concentrations of < 0.1 wt.% AVS-Fe and < 0.15 wt.% CRS-Fe, respectively (Figs. 2b, c). At all Smeerenburgfjorden stations, Fe_{HR}/Fe_T ratios are in the range of 0.18 to 0.38, with a trend of lower values seaward; Fe_{HR}/Fe_T is mostly between 0.26 and 0.31 in Kongsfjorden sediments and > 0.4 at the Van Keulenfjorden sites (Fig. 3a). Fe_{HR}/Fe_T values for Smeerenburgfjorden and Kongsfjorden sediments are thus typical for siliciclastic continental margin sediments (0.28 ± 0.06; Raiswell and Canfield, 1998); Van Keulenfjorden sediments

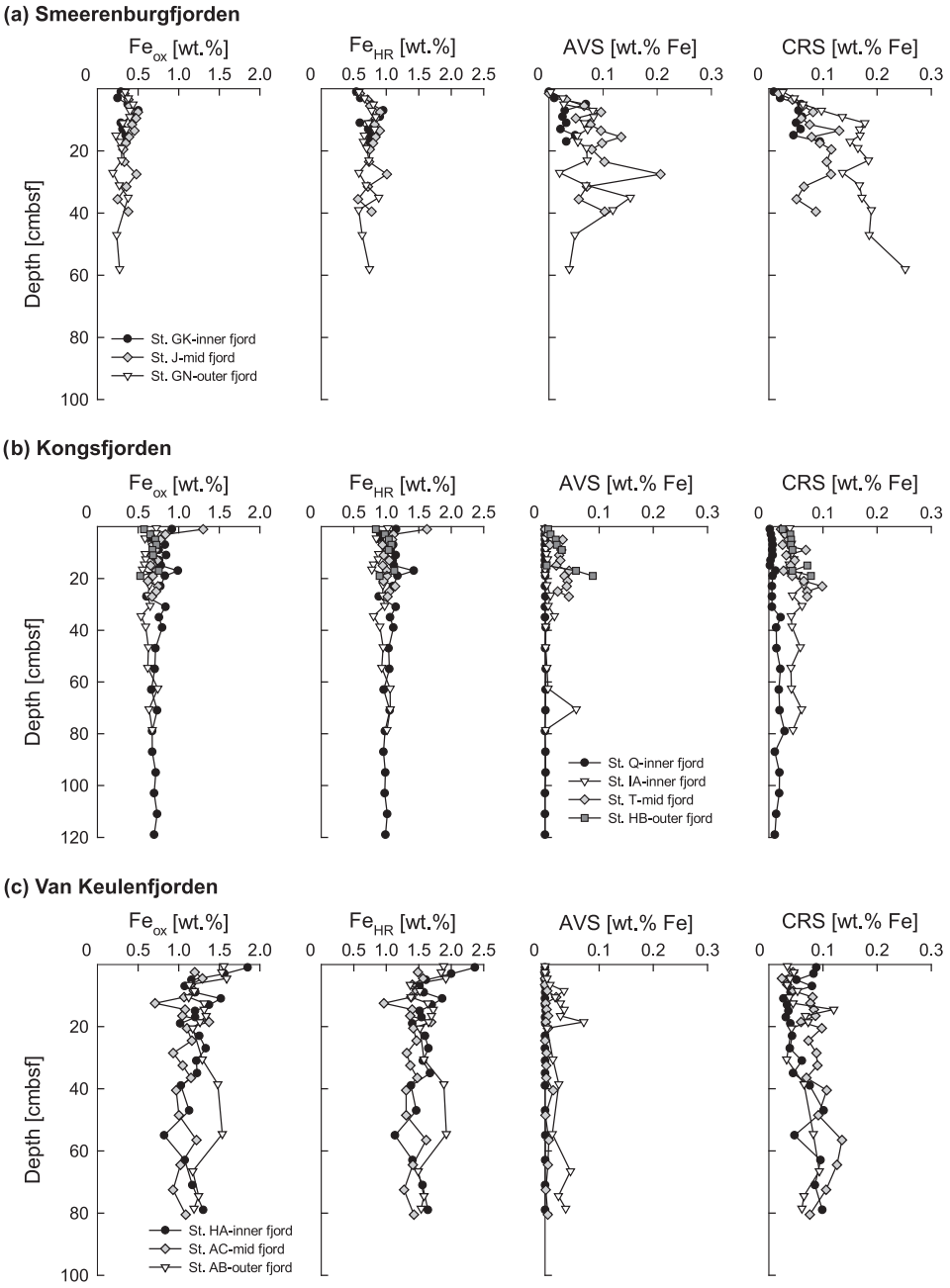

Fig. 2. Concentrations of reducible iron phases (Fe_{ox}; determined by ascorbic acid and dithionite extractions), total amount of highly reactive iron (Fe_{HR}), concentrations of acid volatile sulfide (AVS), and concentrations of chromium reducible sulfur (CRS) at (a) Smeerenburgfjorden Stations GK, J, and GN, (b) Kongsfjorden Stations Q, IA, T, and HB, and (c) Van Keulenfjorden Stations HA, AC, and AB.

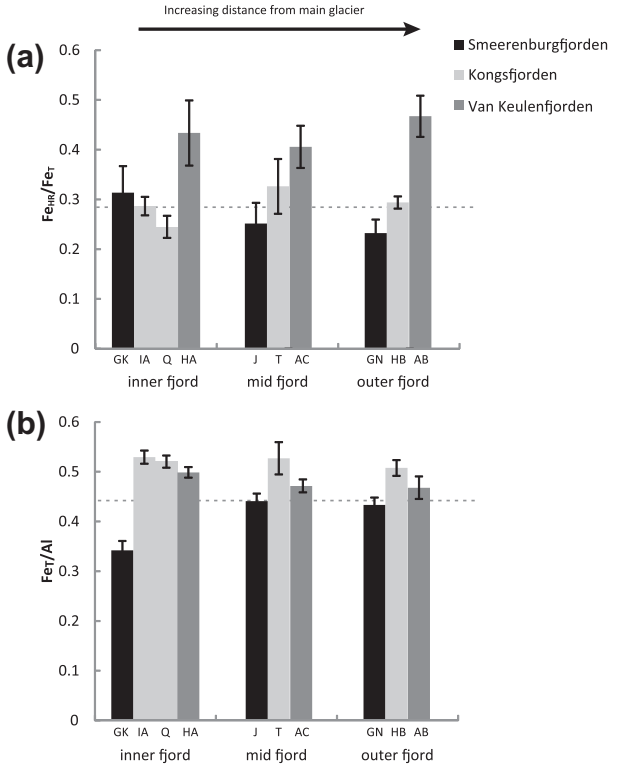

Fig. 3. (a) Total highly reactive iron over total iron ratio (Fe_{HR}/Fe_T) at the inner fjord stations (GK, IA, Q, HA), the mid fjord stations (J, T, AC), and the outer fjord stations (GN, HB, AB). The dotted line represents the average Fe_{HR}/Fe_T of siliciclastic continental margin sediment (0.28; Raiswell and Canfield, 1998). (b) Total iron to total aluminum ratio (Fe_T/Al) at the same fjord stations. The dotted line represents the average crust Fe_T/Al ratios of 0.44 proposed by Taylor and McLennan (1984).

display distinctly higher Fe_{HR}/Fe_T values. Fe_T/Al ratios in Smeerenburgfjorden sediments average 0.34 at inner fjord Station GK and show a trend to values of 0.43–0.44 further down the fjord, which is in the range of average crust Fe_T/Al ratios of 0.44 (Taylor and McLennan, 1985; Fig. 3b). Fe_T/Al ratios of Kongsfjorden and Van Keulenfjorden sediments average 0.51–0.54 and 0.46–0.50, respectively (Fig. 3b). Iron accumulation rates in the Western Svalbard fjords are in the range of 0.9–60 g cm^{-2} kyr^{-1} and generally decrease downfjord (Table 3).

The concentrations of Mn_{extr} at all stations are one order of magnitude lower than iron concentrations determined using the same extraction method. Smeerenburgfjorden sediments contain < 0.015 wt.% Mn_{extr} (Fig. 4a). Van Keulenfjorden sediments show distinct enrichments in Mn_{extr} in the surface sediment compared to the other stations (Fig. 4c), with maximum values at 2.5–5 cm below seafloor (cmbsf) (Fig. 4c).

Similar to the solid-phase iron data, the sedimentary carbon and nitrogen data reveal large differences between the three fjords (Fig. 5). Sedimentary TIC concentrations range from 0.3–0.6 wt.% (Fig. 5a) in Smeerenburgfjorden, between 1.4 wt.% (Station Q) and 2.8 wt.% (Station IA) in Kongsfjorden (Fig. 5a), and are mostly <1 wt.% in Van Keulenfjorden (Fig. 5a). Sedimentary TOC values in Smeerenburgfjorden sediments range from 0.7 to 1.4 wt.% (Fig. 5b). Total organic carbon concentrations range from 0.4 to 1.2 wt.% in Kongsfjorden (Fig. 5b) and are in the range of 1.5–1.8 wt.% in Van Keulenfjorden (Fig. 5b). In all fjords, the glacier-adjacent stations are characterized by the lowest TOC values (Fig. 5b). Molar C/N ratios average 9.3–9.5 at all Smeerenburgfjorden stations (Fig. 5c). Ratios determined for Kongsfjorden Station Q are in the range of 14.8, and those at Station HB average 10.1 (Fig. 5c). In contrast, Van Keulenfjorden sediments display much higher C/N ratios averaging 15.8 (Fig. 5c).

The sulfur isotope compositions of AVS and CRS at the Smeerenburgfjorden sites generally show very similar trends toward heavier values with increasing burial depth (Fig. 6a). Due to the very low AVS concentrations, only a few isotope values were measured for the Kongsfjorden and Van Keulenfjorden stations. Nonetheless, all stations in these fjords show an offset between the sulfur isotope compositions of AVS and CRS of ~10 ‰ (Station AB) and up to 30 ‰ (Station Q), with the AVS being consistently heavier relative to the CRS (Figs. 6b, c).

4.2. Porewater composition

Distinct trends in the porewater profiles of sulfate, iron, and manganese can be highlighted amongst the three fjords.

Table 3
Sedimentation rates for stations sampled in Smeerenburgfjorden (from Hubert et al., 2009 and Heggdal Velle, 2012) and Van Keulenfjorden (Kempf et al., 2013), as well as sediment accumulation rates for Kongsfjorden (Svendsen et al., 2002). These data are used to calculate iron accumulation rates for these stations.

Fjord	Station	Sedimentation rate [cm yr^{-1}]	Sediment accumulation rates [g cm^{-2} yr^{-1}]	Fe accumulation rate [g cm^{-2} kyr^{-1}]
Smeerenburgfjorden	GK	0.44		11.5
	J	0.19		4.2
	GN	0.03		0.9
Kongsfjorden	IA		1.84	60
	T		0.18	6.1
Van Keulenfjorden	AC	0.06		2.2
	AB	0.08		3.5

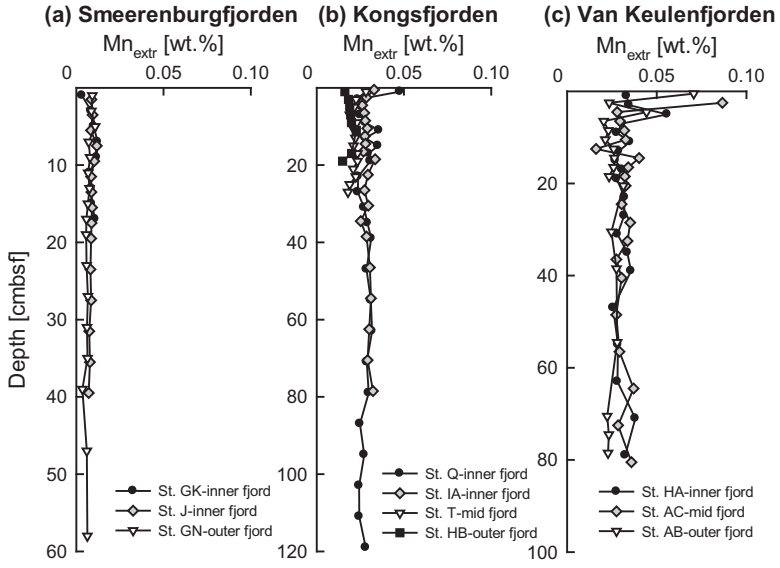

Fig. 4. Total extractable manganese (Mn_{extr}) concentrations in the sediment of (a) Smeerenburgfjorden, (b) Kongsfjorden, and (c) Van Keulenfjorden stations.

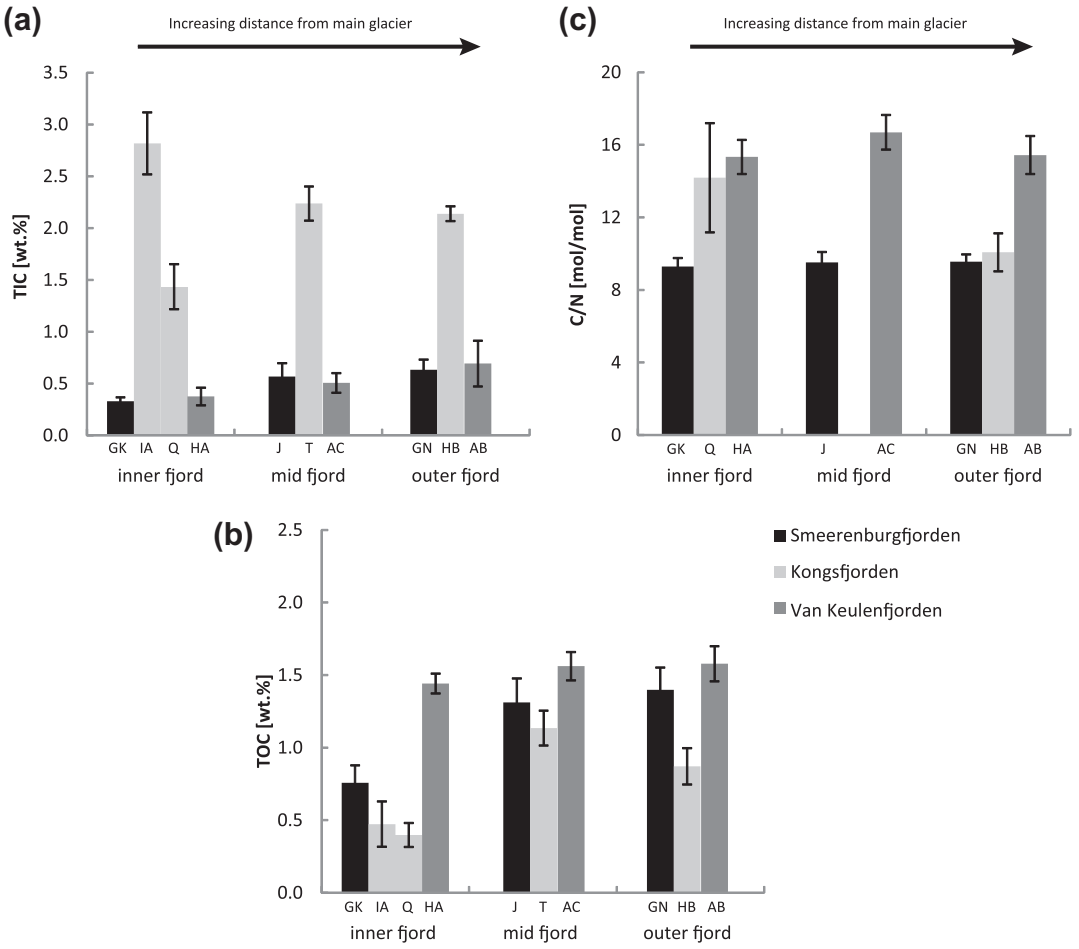

Fig. 5. (a) Sedimentary total inorganic carbon (TIC) concentrations, (b) total organic carbon (TOC) concentrations, (c) and TOC to total nitrogen ratios (C/N) at the inner fjord stations (GK, IA, Q, HA), the mid fjord stations (J, T, AC), and the outer fjord stations (GN, HB, AB).

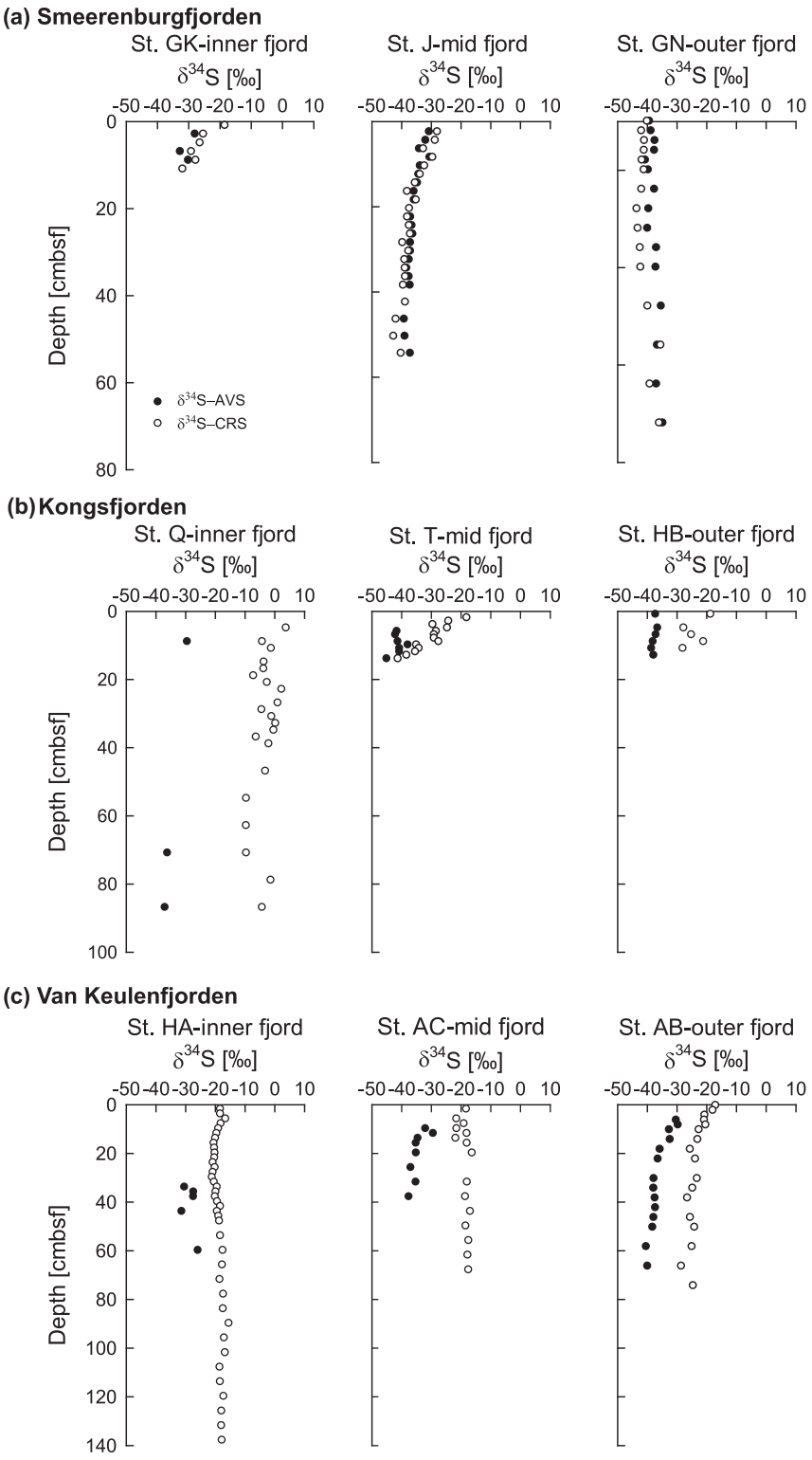

Fig. 6. Sulfur isotope composition of acid volatile sulfide (AVS) and chromium reducible sulfur (CRS) in (a) Smeerenburgfjorden, (b) Kongsfjorden, and (c) Van Keulenfjorden sediments.

First, sulfate concentration profiles display pronounced decreases with depth only at the Smeerenburgfjorden sites J and GN (Fig. 7a), while sulfate concentrations at the Kongsfjorden and Van Keulenfjorden stations vary less than 2 mM (Fig. 7b and c). Hydrogen sulfide concentrations at Smeerenburgfjorden Station GK and at all stations

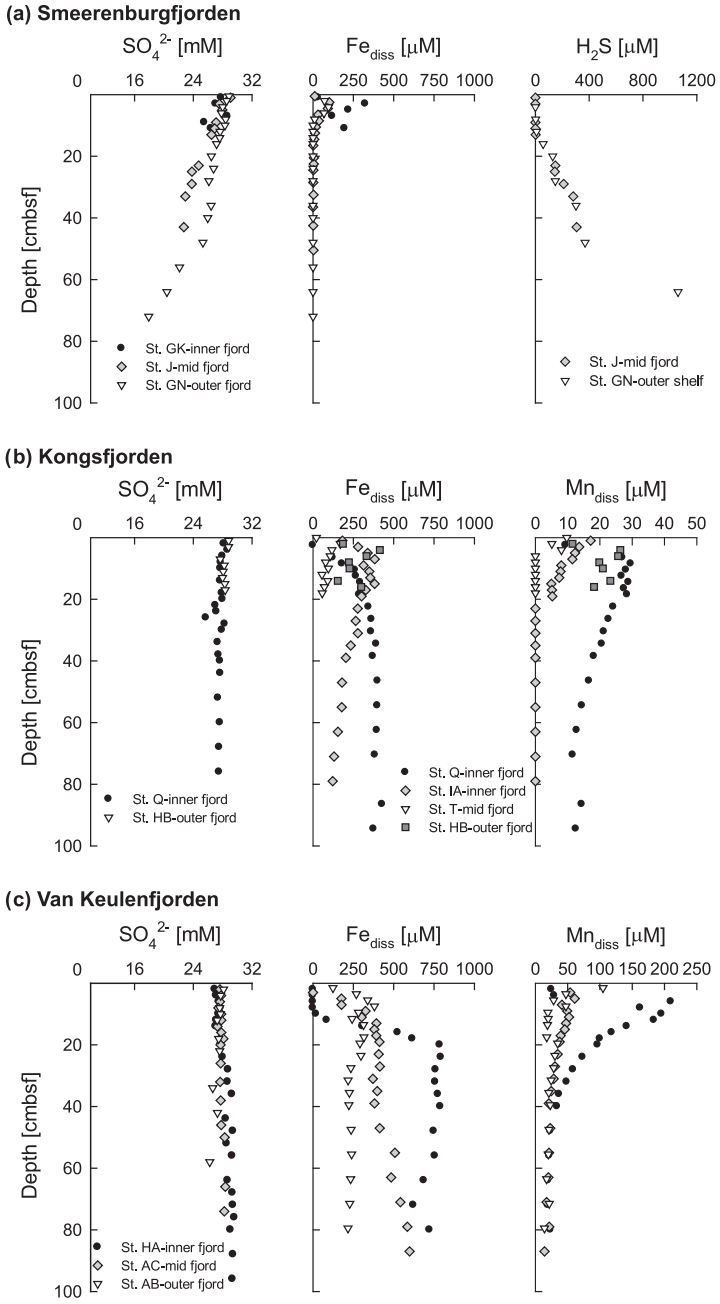

Fig. 7. (a) Porewater sulfate (SO_4^{2-}), dissolved iron (Fe_{diss}) and hydrogen sulfide (H_2S) concentrations in Smeerenburgfjorden sediments, (b) SO_4^{2-}, Fe_{diss} and dissolved manganese (Mn_{diss}) concentrations in Kongsfjorden and (c) in Van Keulenfjorden sediments.

in Kongsfjorden and Van Keulenfjorden are below detection limit. They reach values of up to 306 µM at 43 cmbsf at Station J and 1060 µM at 64 cmbsf at Station GN, respectively (Fig. 7a).

Porewater iron is only present in the top 8 cm of Smeerenburgfjorden Stations J and GN, with maximum values of 91 and 127 µM, respectively (Fig. 7a). In contrast, porewater iron concentrations at the inner Smeerenburgfjorden Station GK and the Kongsfjorden stations reach maximum values of up to 415 µM (St. HB) in the top 10 cm of the sediment and display only slight decreases in concentration below (Fig. 7b). At the Van Keulenfjorden stations, iron concentrations are below detection in the surface sediment, increase sharply to a maximum value of 793 µM (Station HA) at 8–20 cmbsf, and stay in this range over the remaining core depth (Fig. 7c).

Porewater manganese concentrations at Smeerenburgfjorden Station GK range from 18 to 32 µM and are mostly below detection at Stations J and GN (data not shown). At the Kongsfjorden stations, manganese concentrations reach maximum values of up to 30 µM in the top 6–8.5 cm of the sediments and decrease below to values below detection at

Table 4
Dissolved iron (Fe) fluxes towards the oxygenated surface sediment based on the REC model (Lettmann et al., 2012) and dissolved iron fluxes across the sediment–water interface calculated according to Raiswell and Anderson (2005). Also shown are dissolved manganese (Mn) fluxes towards the oxygenated surface layer based on the REC model.

Fjord	Station	Dissolved Fe flux towards the oxygenated surface layer [μmol m^{-2} d^{-1}]	Dissolved Fe flux across the sediment–water interface [μmol m^{-2} d^{-1}]	Dissolved Mn flux towards the oxygenated surface layer [μmol m^{-2} d^{-1}]
Smeerenburgfjorden	GK	400	47	23
	J	50	42	n.d.
Kongsfjorden	Q	78	0	12
	IA	91	n.d.	n.d.
	T	196	13	n.d.
	HB	317	48	19
Van Keulenfjorden	HA	3	0	80
	AC	157	0	10
	AB	185	131	n.d.

Stations IA and T (Fig. 7b). Highest manganese concentrations were measured at the Van Keulenfjorden stations, reaching values of up to 210 μM (Station HA) in the top 6 cm and showing a pronounced decrease below (Fig. 7c).

Calculated fluxes of dissolved iron toward the oxygenated sediment surface layer range from 2.6 μmol m^{-2} d^{-1} at Station HA to 400 μmol m^{-2} d^{-1} at Station GK (Table 4; Fig. 8a). In Smeerenburgfjorden, the glacier-adjacent Station GK shows the highest iron flux toward the oxygenated surface sediment, while in Kongsfjorden and Van Keulenfjorden, a trend toward increased iron fluxes with increasing distance from the glaciers at the fjord heads can be noted (Table 4; Fig. 8a). Calculated iron fluxes across the sediment–water interface fall in a similar range of ~45 μmol m^{-2} d^{-1} for Smeerenburgfjorden Stations J and GK (Fig. 8a). No iron fluxes across the sediment–water interface could be calculated for the innermost Kongsfjorden and Van Keulenfjorden stations since surface iron concentrations are below detection. For the outermost Stations HB and AB, derived flux values are 48 and 125 μmol m^{-2} d^{-1}, respectively. For most stations, the iron flux values across the sediment–water interface are around one order of magnitude lower than those calculated toward the oxygenated surface sediment using the REC model (Fig. 8a). All inner-fjord stations display fluxes of manganese towards the sediment–water interface of up to 80 μmol m^{-2} d^{-1} (St. HA; Table 4; Fig. 8).

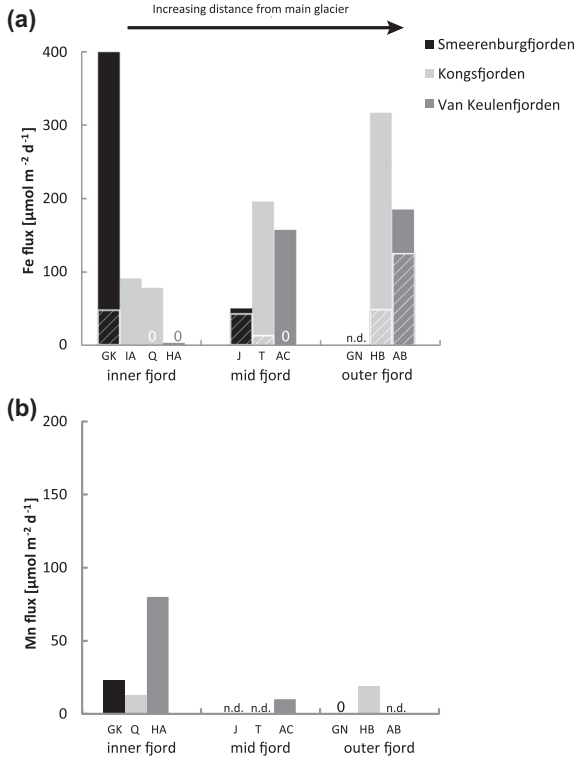

Fig. 8. (a) Calculated fluxes of dissolved iron towards the oxygenated surface sediment (full columns) based on the REC model (Lettmann et al., 2012) and dissolved iron fluxes across the sediment–water interface (shaded columns, zeros) calculated according to Raiswell and Anderson (2005). (b) Calculated fluxes of dissolved manganese towards the oxygenated surface sediment based on the REC model.

5. DISCUSSION

5.1. The effect of bedrock composition and glacial regime on the input of glacially derived particulate iron and organic matter to fjord sediments

Differences with respect to reducible iron concentrations and Fe_{HR}/Fe_T and Fe_T/Al ratios amongst the three western Spitsbergen fjords (Figs. 2 and 3) can be attributed to differences in the local bedrock geology below the main glaciers and weathering processes associated with the glacial regime (Fig. 9). The composition of the subglacial basement rock controls the quantities and qualities of the reducible iron phases that are mechanically weathered as rock flour and the amount of pyrite available for the subglacial pyrite-oxidizing microbial community. Bedrock lithologies poor in total iron and pyrite in the Smeerenburgfjorden area, such as granites and gneiss, produce low-iron glacial flour. In contrast, mechanical weathering of the Van Keulenfjorden arenaceous sandstones likely delivers a higher iron component, which may additionally be enriched in iron (oxyhydr)oxides due to the occurrence of pyrite oxidation below the local glaciers. Wadham et al. (2004, 2007,

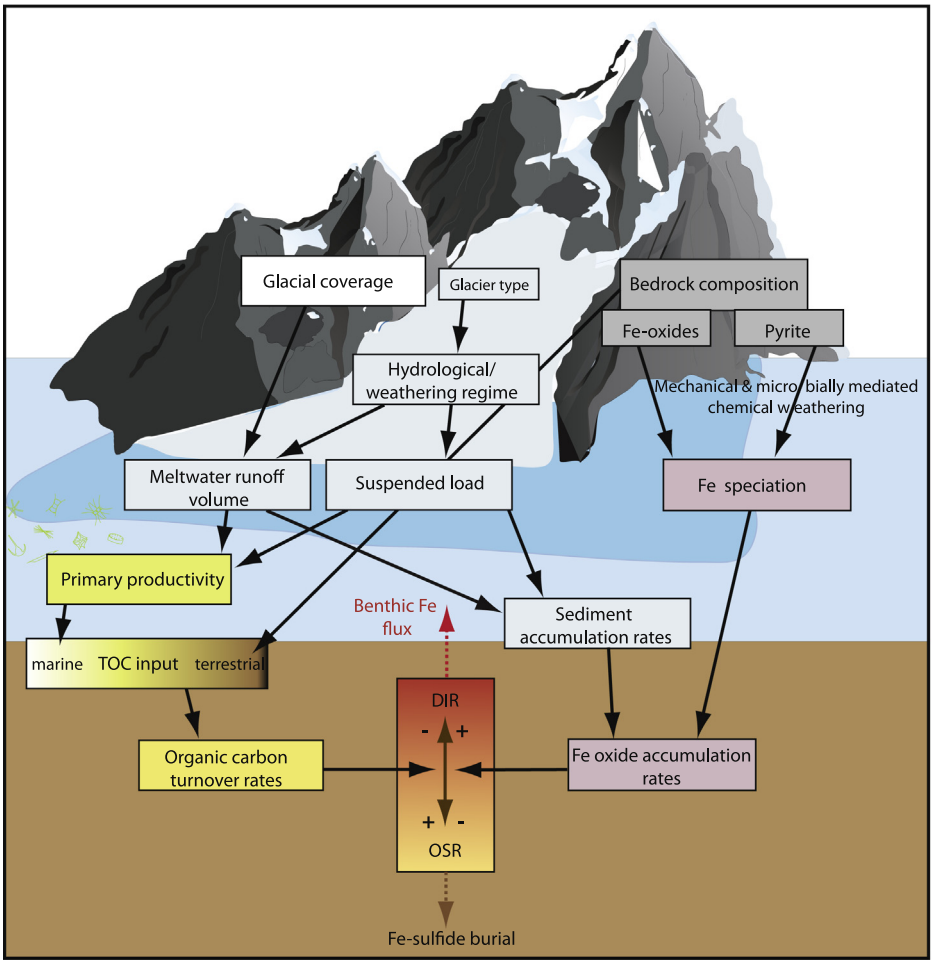

Fig. 9. Summary schematic showing the major processes and features that influence the input of organic matter and iron oxide phases to fjord sediments, and their effects on the occurrence of dissimilatory iron reduction (DIR) and organoclastic sulfate reduction (OSR).

2010) found evidence for the occurrence of microbial sulfide oxidation in the proglacial zone and glacier beds of Finsterwalderbreen, a large glacier on the southern coast of Van Keulenfjorden, and accordingly, Poulton and Raiswell (2005) determined a high Fe_{HR}/Fe_T ratio of 0.70 for the fine fraction (<2 μm) of Finsterwalderbreen runoff. Meltwater residence times for the glaciers of both Kongsfjorden (Midre Lovénbreen) and Van Keulenfjorden (Finsterwalderbreen) are sufficiently long to allow for substantial pyrite oxidation (Hodson and Ferguson, 1999; Glasser and Hambrey, 2001; Brown, 2002; Tranter et al., 2005; Skidmore et al., 2010; Wadham et al., 2010), likely contributing to the elevated reducible iron (oxyhydr)oxide concentrations observed in the respective fjords. The composition of the catchment bedrock may also influence the input of extractable manganese phases, which show low values in Smeerenburgfjorden sediments and higher values for Kongsfjorden and Van Keulenfjorden sediments (Fig. 4).

The Fe_{HR}/Fe_T values for all three fjord sediments are higher than for most previously analyzed glacial sediments (meltwater or subglacial), e.g., the French Alps and Antarctica (Poulton and Raiswell, 2005; Raiswell et al., 2006). This additional mechanism that enriches the sediments with Fe_{HR} phases and contributes to a characteristic glacially derived highly reactive iron component, particularly in Van Keulenfjorden sediments, may result from a size-sorting of the meltwater particulate phase during passage across the proglacial zones of glaciers. Coarser grains, which often have low Fe_{HR}/Fe_T values (Poulton and Raiswell, 2005; Raiswell et al., 2006; Roy et al., 2013), settle out along the proglacial areas, while dissolved and fine-grained particulate iron phases remain in the meltwater and enter the fjord.

The concentration and stable sulfur isotope composition of CRS suggest that the sedimentary pyrite pools of Kongsfjorden and Van Keulenfjorden sediments include large fractions of fine-grained detrital pyrite transported from mechanical weathering of basement rock below the glaciers. The relatively high and constant concentration of CRS in the top 10 cm (Figs. 6b, c), where dissimilatory metal reduction rather than organoclastic sulfate reduction prevails, provides a first indication that this CRS is not formed *in situ*. Furthermore, the CRS sulfur isotope compositions at both fjords are decoupled (10 to 30‰ offset) from the

AVS isotope composition at similar sediment depth. The AVS is assumed to form *in situ* since these phases are only stable for short time periods in marine sediments before they are re-oxidized or transformed further to CRS (see Schoonen, 2004; Jørgensen and Kasten, 2006; and references therein). If the CRS pool also predominately formed *in situ*, it would have an isotopic value closer to or more negative than the AVS value, as for example seen at Smeerenburgfjorden Station GN. The most positive $\delta^{34}S$ values of CRS are observed at the inner fjord and mid-fjord stations, consistent with a detrital input.

The delivery of mechanically and chemically derived glacial debris, and thus the sedimentation rate in the adjacent fjords, is controlled mainly by the runoff volume and suspended load of the local glaciers. Sedimentation rates can reach several centimeters to meters per year (see Howe et al., 2010, for review). For example, in the inner Kongsfjorden area, Trusel et al. (2010) measured sedimentation rates of up to 30 cm per year. Iron accumulation rates calculated for the inner Smeerenburgfjorden Station GK and the inner Kongsfjorden Station IA are 11.5 and 60 g cm^{-2} kyr^{-1}, respectively, and we can assume that the iron accumulation rate at inner Van Keulenfjorden Station HA is in a similar range—considering the large glaciers entering this fjord. These iron accumulation rates in the Svalbard fjords are in the same range as those of a riverine estuary of similar size, e.g., the Medway Estuary, UK (Spencer et al., 2003), and the slightly larger Barataria Estuarine Basin, Louisiana, USA (Feijtel et al., 1988). Changes in iron accumulation rates and thus potentially rates and pathways of biogeochemical processing in associated fjord sediments can be expected as a function of variation in the volume and suspended load of glacial runoff. Smeerenburgfjorden is influenced by only one main tide water glacier, Smeerenburgbreen, which is much smaller than several of the glaciers entering Kongs- and Van Keulenfjorden and has a significantly smaller catchment area (Table 1). It is likely that the small-sized glacier in Smeerenburgfjorden has a lesser influence on fjord biogeochemistry, particularly away from the fjord head, compared to the glaciers in Kongsfjorden and Van Keulenfjorden (Fig. 9).

The meltwater volume and suspended load of glacial runoff also affect primary productivity in the water column and the input of organic matter to fjord sediments by suppressing conditions suited to primary producers. High sediment loads in meltwater plumes strongly reduce the penetration depth of sunlight in the water column and thus limit primary production to a narrow surface zone of 0.3 m or less (e.g., Hop et al., 2002). Low salinity meltwaters often prove detrimental for marine zooplankton, leading to reduced zooplankton numbers in the water column adjacent to the glaciers (Zajaczkowski and Legezynska, 2001; Hop et al., 2002). Surface waters in Kongsfjorden and Van Keulenfjorden were very turbid compared to Smeerenburgfjorden, which had clear surface waters during both sampling campaigns. Turbidity and freshwater effects thus likely prevail in the inner and central Kongsfjorden and Van Keulenfjorden areas due to the high meltwater runoff rates of glaciers in these fjords but are limited to the inner-fjord of Smeerenburgfjorden. The high sediment input and low primary productivity contribute to the low TOC content of the glacier-adjacent sites, such as GK and Q (Fig. 5).

Intriguingly, TOC values are highest in Van Keulenfjorden sediments (Fig. 5b), although based on the argument above it might be predicted that primary production is overall higher in Smeerenburgfjorden surface waters than in the other fjords due to the lower meltwater runoff. The sedimentary C/N ratios, which display distinct differences among the three fjords (Fig. 5c), can be used to distinguish between different organic matter sources (e.g., Hebbeln and Berner, 1993; Wagner and Dupont, 1999), although the adsorption of inorganic nitrogen on illite phases may distort C/N ratios towards lower values in Arctic sediments (Schubert and Calvert, 2001; Winkelmann and Knies, 2005). Smeerenburgfjorden sedimentary C/N ratios are close to typical marine phytoplankton-derived organic matter (4–10; Meyers, 1994), suggesting that the available organic matter was produced within the fjords or brought in from the adjacent shelf and may be relatively unaltered. Van Keulenfjorden C/N ratios of >16 and Kongsfjorden ratios reaching 14 suggest contributions from sources other than "fresh" marine phytoplankton. It is likely that these elevated C/N ratios derive in part from the input of terrestrial organic matter (C/N ratios >20) from glacial erosion and river runoff. However, since the Kongsfjorden and Van Keulenfjorden areas are heavily glaciated, and few ice-free spots provide favorable conditions for plant growth (Winkelmann and Knies, 2005), most of the terrestrial organic matter is probably brought in from below the glaciers and is thus likely to be diagenetically altered and reworked (e.g., Premuzic et al., 1982; Meyers, 1994). Similarly, indices for chlorophyll- and amino acid-derived degradation suggest that the organic matter in Smeerenburgfjorden surface sediments is less altered than in Kongsfjorden and is possibly more available for microbial diagenesis (Ahke, 2007). The more pristine marine organic matter in Smeerenburgfjorden sediments likely results in higher TOC mineralization rates, and thus elevated consumption rates of terminal electron acceptors, compared to sediments in Kongsfjorden and Van Keulenfjorden.

5.2. Biogeochemical processes in fjord sediments

The varying glacier-controlled input of reducible iron and manganese oxide phases and organic matter of different alteration states control the pathways of organic carbon mineralization in the sediments of the three fjords. Nearly constant sulfate concentrations and elevated dissolved manganese and iron concentrations of up to 800 μM were present in the porewaters at all Kongsfjorden and Van Keulenfjorden stations down to the maximum coring depth of 120 cmbsf (Fig. 7a-c). The greatly elevated dissolved iron and manganese concentrations in the porewaters may result from dissimilatory metal reduction of the iron (oxy-hydr)oxide and manganese oxide phases (Lovley, 1991, 1997; Nealson and Myers, 1992), although a fraction of the dissolved metals may also derive from the oxidative cycling of intermediate sulfur species produced during

organoclastic sulfate reduction and coupled to iron and manganese oxide reduction (Aller et al., 1986; Brüchert et al., 2001; Berg et al., 2003). Previous studies in Western Svalbard fjords noted a substantial contribution by dissimilatory iron reduction (DIR) to organic matter mineralization (10–43%; Kostka et al., 1999; Vandieken et al., 2006a,b), similar to other coastal areas (e.g., Canfield et al., 1993b; Jensen et al., 2003). Dissimilatory metal reduction in the fjord sediments may be sustained by the high metal delivery rates and the occurrence of bioturbation and/or bioirrigation (Jørgensen et al., 2005; Hubert et al., 2009), which lead to continuous re-oxidation of dissolved iron and manganese species (Aller et al., 1986; Canfield et al., 1993a,b; Alongi, 1995; Aller and Aller, 1998). Past observations suggest that bioturbation and bioirrigation are more prevalent in central and outer fjord stations (e.g., Glud et al., 1998; Kostka et al., 1999) and are lower close to the glaciers where the very high sedimentation rates and the low organic matter contents result in low biomass and low diversity of the macrofauna (Holte et al., 1996; Hop et al., 2002). Inner fjord Stations HA and IA show the highest porewater metal concentrations amongst the Van Keulenfjorden and Kongsfjorden stations (Fig. 7). At these stations, the physical process of iceberg scouring may contribute to sediment dispersion and likely promotes dissolved (aqueous and nanoparticulate) metal re-oxidation close to the glaciers.

Subtle decreases in sulfate concentrations and small increases in sedimentary AVS concentrations with depth at the mid- and outer Kongsfjorden and Van Keulenfjorden stations (Figs. 2 and 7) indicate the occurrence of low rates of sulfate reduction coupled to the oxidation of organic matter (organoclastic sulfate reduction). This process, however, is likely confined to the sediment below the top 20 cm; in the shallow layers, continuous benthic recycling primarily drives dissimilatory metal reduction. The produced hydrogen sulfide reacts with dissolved iron in the porewater to form AVS and CRS but may also undergo re-oxidation to sulfate and intermediate sulfur species (Berner, 1970; Berner and Raiswell, 1984; Aller et al., 1986; Raiswell and Canfield, 1998).

In contrast to Kongsfjorden and Van Keulenfjorden, depth profiles at Smeerenburgfjorden Stations GN and J display porewater iron maxima in the top 10 cm of the sediment and pronounced decreases in sulfate concentrations accompanied increasing hydrogen sulfide concentrations below the top iron-rich (ferruginous) layer (Fig. 7a). These data indicate that DIR in this fjord is likely confined to the top cm of the sediment, while organic carbon mineralization in the remaining sediment column is predominantly driven by organoclastic sulfate reduction (Vandieken et al., 2006a). In Smeerenburgfjorden sediments, AVS and CRS are mostly formed *in situ*, and the $\delta^{34}S$ values of AVS and CRS are thus very similar (Fig. 6). Higher organic carbon mineralization rates and lower reducible iron oxide input favor the occurrence of organoclastic sulfate reduction over DIR, thus sulfate reduction rates in Smeerenburgfjorden are twice as high as those determined for Kongsfjorden (Ahke, 2007). Nonetheless, the production of a thin layer of DIR in the top 1–5 cm of the surface sediment yields a substantial flux of dissolved iron into the overlying water column in the inner and mid Smeerenburgfjorden areas (Stations GK and J; Fig. 8a).

5.2.1. The role and biogeochemical cycling of iron and manganese in Kongsfjorden and Van Keulenfjorden sediments

Dissolved iron and manganese in Kongsfjorden and Van Keulenfjorden porewaters reach the overlying oxic surface waters by diffusion, bioirrigation, bioturbation, and physical mixing of surface sediments (e.g., Aller et al., 1986; Elrod et al., 2004; Raiswell and Anderson, 2005; Homoky et al., 2012). Pronounced peaks in the porewater distribution of dissolved manganese in the top cm at Station Q in Kongsfjorden and Station HA and Station AC in Van Keulenfjorden, followed by prominent increases in iron concentrations below the surface layers (Figs. 5b and c), indicate a distinct biogeochemical zonation separating manganese and iron oxide reduction. Such a confined zonation is commonly explained by the higher energy yield of dissimilatory manganese reduction compared to iron reduction (e.g., Froelich et al., 1979) and the reaction of dissolved iron with manganese oxides (Burdige and Nealson, 1986; Myers and Nealson, 1988; Burdige, 1993; Canfield et al., 1993a). As a result of the prevalent role of dissimilatory manganese reduction at the inner-fjord stations HA and Q, calculated fluxes for manganese exceed those for iron, and oxidation of aqueous iron by manganese oxides contributes to the limited flux of iron across the sediment–water interface. The calculated manganese fluxes of up to 80 $\mu mol\ m^{-2}\ d^{-1}$ at these stations exceed those of typical shelf-to-shallow margin sites by an order of magnitude ($8 \pm 5\ \mu mol\ m^{-2}\ d^{-1}$; McManus et al., 2012) but are in a similar range as fluxes calculated for the non-glaciated Gullmarsfjorden, Sweden ($93\ \mu mol\ m^{-2}\ d^{-1}$; Sundby et al., 1986). Extractable manganese phases are enriched in the surface sediment layers at Stations HA and Q (Fig. 3b, c); similar surface manganese enrichments have previously been described for Arctic Ocean sediments by Gobeil et al. (1997) and Macdonald and Gobeil (2012). The enrichments are the result of manganese re-oxidation at the sediment surface. Dissolved manganese diffusing into the water column also readily adsorbs onto particles, but a fraction of it is released into the water column (Richard et al., 2013).

The data from the Kongsfjorden and Van Keulenfjorden transects reveal that with increasing distance from the glaciers, the porewater manganese maxima are located closer to the sediment–water interface (Fig. 7). This relationship is likely due to seaward decreases in sedimentation rates and increases in mineralization rates facilitated by higher inputs of marine organic matter, as evidenced by the seaward increase in TOC values in all fjords and a decline in C/N ratios, particularly in Kongsfjorden (Fig. 5). The increase in mineralization rates results in a thinning of the zone of aerobic respiration and manganese reduction and may aid the escape of manganese into the overlying water column. Our results support previous studies, which suggest that the diagenetic recycling of manganese in coastal Arctic sediments is an important pathway that contributes to the delivery of manganese to the water column and subsequent transport to adjacent slope and

basin sedimentary sequences (Macdonald and Gobeil, 2012; März et al., 2011, 2012).

Fluxes of porewater iron towards the surface oxidizing layer of the sediment calculated for the Svalbard fjord sediments reach values of up to 317 and 400 μmol m^{-2} d^{-1} at outer Kongsfjorden Station HB and inner Smeerenburgfjorden Station GK, respectively, and are mostly between 70 and 190 μmol m^{-2} d^{-1} at the other stations (Table 4; Fig. 8). In contrast to manganese, the porewater iron concentration gradients—and thus the fluxes—of iron towards the surface sediment increase with increasing distance from the glaciers in Kongsfjorden and Van Keulenfjorden. However, not all of the dissolved iron diffusing towards the sediment–water interface reaches the overlying waters, as a fraction of it is oxidized by oxygen, nitrate, or manganese oxides in the top oxic sediment layer. Calculated porewater iron fluxes based on porewater iron profiles may overestimate real iron flux values if iron precipitation in the shallow surface sediment is not adequately quantified. Employing the approach of Raiswell and Anderson (2005) and Homoky et al. (2012), we calculated adjusted iron flux estimates of up to 125 μmol m^{-2} d^{-1}. Thus, despite the removal of some iron by oxide precipitation, aqueous iron escapes across the oxygenated sediment surface layer to the overlying water column at most sites (Table 4; Fig. 8).

Comparable iron fluxes have so far only been reported from a few sites along the Northern Oregon-California shelf, the San Pedro and Santa Monica basins, and other areas where bottom water oxygen concentrations are low (Sundby et al., 1986; Elrod et al., 2004; Pakhomova et al., 2007; Severmann et al., 2010). Our data suggest that despite the high levels of bottom water oxygen in Svalbard fjords in the range typical of polar surface waters (>330 mmol m^{-3}; Sarmiento and Gruber, 2006), the high porewater iron levels, aided by bioturbation and physical mixing of surface sediments, and low bottom water temperatures, which slow oxidation kinetics, may allow for a significant benthic iron flux averaging 55 μmol m^{-2} d^{-1} from fjord sediments.

5.3. Transport and potential bioavailability of glacially derived iron in fjords

Dissolved (aqueous and nanoparticulate) iron, originating from the diagenetic recycling of iron in fjord sediments, will be partially re-oxidized to form new nanoparticulate and particulate iron (oxyhydr)oxide phases in the oxic bottom waters (Raiswell and Canfield, 2012), or it will adsorb onto particulate iron and manganese phases (Homoky et al., 2012; Richard et al., 2013). These iron oxidation processes at or near the sediment–water interface contribute to the formation of distinct layers enriched in easily reducible iron, such as in the top cm of most Van Keulenfjorden and some Kongsfjorden sediments (Fig. 2b and c). Bottom currents may also entrain, vertically mix, and export the diagenetically produced dissolved and particulate iron phases in fjord bottom waters into the upper water column. This mechanism has been described previously for other continental margin sites (Johnson et al., 1999; Elrod et al., 2004; Raiswell and Anderson, 2005; Lyons and Severmann, 2006; Severmann et al., 2010; Siedlecki et al., 2012). Depending on the season, different oceanographic processes may drive this transport, as outlined here for Kongsfjorden (Fig. 10). From late spring to

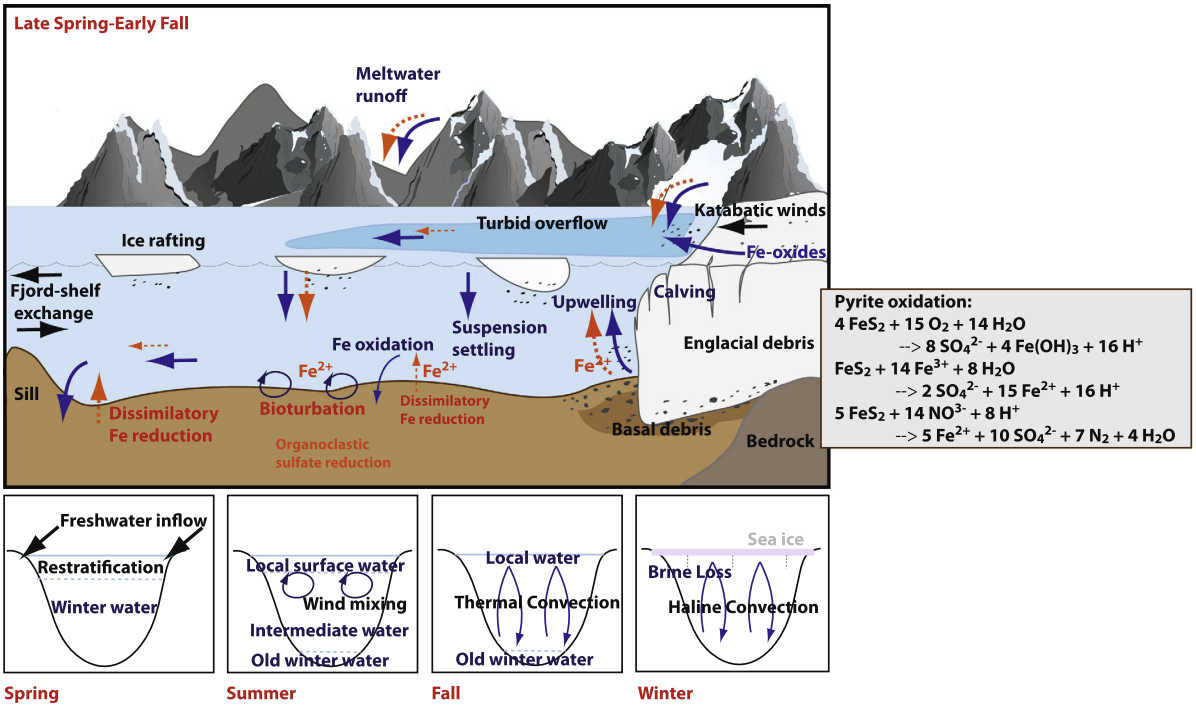

Fig. 10. Conceptual figure depicting the major sources of dissolved iron (orange) and particulate iron phases (blue) to fjord waters and sediments, the biogeochemical cycling of iron in the fjord sediments, and transport pathways of iron seaward (adapted from Howe et al., 2010). Also shown is the seasonal cycle of stratification in Svalbard fjords adapted from Cottier et al. (2010), including the substantial seasonal freshwater input (FW) during spring melt.

early fall, intermediate to deep water masses enter Kongsfjorden along the southern coast as an internal Kelvin wave in a well-established pattern driven primarily by tidal and coastal wind forcing and exit the fjord along the northern shore (Svendsen et al., 2002; Cottier et al., 2005). This internal wave can pick up diagenetically derived iron phases in the bottom water and deliver them to the adjacent shelf. In some fjords, the presence of a sill at the fjord mouth, however, may limit exchange of deep water, formed during the past winter, during the following spring and summer (Fig. 10). Furthermore, in close proximity to the local glaciers, mixing between brackish water entering the fjord from below the glaciers and fjord water causes buoyancy-driven upwelling of deep waters that can re-suspend particles from the sea bottom into upper water masses, including the brackish overflow layer (Fig. 9; Svendsen et al., 2002; Zajączkowski, 2008). During summer, the strong density stratification in the glacier-fed fjords (Svendsen et al., 2002; Zajaczkowski, 2008; Trusel et al., 2010) may allow for a fraction of fine particles (i.e., silt and clay), which remain in suspension in the brackish overflow layer to be transported directly from the glaciers to the fjord mouth (Fig. 9; Zajączkowski, 2008). In the western Svalbard fjords, surface transport can be strongly enhanced by downfjord (katabatic) winds in summer (Svendsen et al., 2002) and tidal forcing (Fig. 10; Cowan and Powell, 1990; Dowdeswell and Cromack, 1991). Poulton and Raiswell (2005) showed that the finest fractions (<15 μm) of glacial meltwater particulates are strongly enriched in Fe_{HR} and correspondingly have much higher Fe_{HR}/Fe_T ratios compared to coarser particles. In fall and winter, vertical convection processes driven by sea-ice formation and dense brine rejection control mixing in the water column and can lead to the redistribution of diagenetic iron into surface waters (Fig. 10; e.g., Svendsen et al., 2002; Cottier et al., 2010). A fraction of the iron phases in the Svalbard fjords is likely also bound in newly forming sea-ice and subsequently transported to the adjacent shelf when the ice cover breaks in the following spring (May–July; Hölemann et al., 2005; Tovar-Sánchez et al., 2010; Thuroczy et al., 2011). Overall, these chemical and physical mechanisms may facilitate the transport of glacially derived iron phases across the fjords to the adjacent shelf and potentially beyond the shelf break to the open ocean (Fig. 10).

We did not attempt a direct analysis of the bioavailability of the iron in the water column of the Svalbard fjords that originates from glacial runoff and diagenetic recycling in the fjord sediments. Nonetheless, information can be gained from previous studies of these iron phases in similar aquatic environments. Such studies highlight the bioavailability of glacially derived aqueous and colloidal/nanoparticulate iron phases, which have been shown to support phytoplankton growth, for example, in the Amundsen Sea and the Greenland Sea (Statham et al., 2008; Gerringa et al., 2012; Wadham et al., 2013; Bhatia et al., 2013; Lannuzel et al., 2014). An important process that may contribute to the enhanced bioavailability of glacially derived iron is microbially mediated pyrite oxidation below the glaciers, which results in the production of "fresh" aqueous and nanoparticulate iron phases at low pH. Similarly, previous studies have proposed that diagenetically recycled iron from benthic sources represents an important source of dissolved and (nano)particulate iron to the water column (Elrod et al., 2004; Hurst et al., 2010; Severmann et al., 2010). Thereby, the oxidation of porewater Fe(II) creates new nanoparticulate iron(oxyhydr)oxide phases (Raiswell and Canfield, 2012), which are likely initially bioavailable (Chen and Wang, 2001; Chen et al., 2003). Upon entry into the fjord waters, aging and further oxidation of the glacially and benthic derived iron phases result in transformation to more stable particulate phases, e.g., goethite and hematite (Schwertmann et al., 2004), and decrease their bioavailability due to their lower solubility and dissolution rates in the seawater (Rich and Morel, 1990; Yoshida et al., 2006; Bligh and Waite, 2011). However, the rapid formation of organometallic colloids with humic acids weathered from the terrestrial realm, for example, may stabilize these iron phases and maintain their bioavailability (Krachler et al., 2005; Nakayama et al., 2011; Thuroczy et al., 2011, 2012; Gledhill and Buck, 2012). These iron phases can be transported oxically substantial distances offshore, where they may be accessible to phytoplankton on time-scales suitable to support their growth in the surface ocean (Nishioka et al., 2007; Lam and Bishop, 2008; Hurst et al., 2010; de Jong et al., 2013). In the highly productive Svalbard shelf waters, several mechanisms—such as the utilization of specific reductases at the cell surface (Maldonado and Price, 2001; Maldonado et al., 2006), protozoan grazing (Barbeau et al., 1996), viral lysis, bacterial remineralization (Hassler and Schoemann, 2009), and thermal and photochemical processes (Wells et al., 1991; Barbeau et al., 2001; Rijkenberg et al., 2008)—may allow the phytoplankton community to access this iron. It is likely, however, that a fraction of the transported iron, especially larger particulate fractions, also rapidly sinks to the seafloor (Lannuzel et al., 2014).

5.4. Implications of a warming of the Arctic for iron cycling in glacier-fed fjords

The Arctic Ocean is regarded as one of the world's most sensitive regions with respect to global climate change (Anisimov et al., 2007). This region has experienced important changes during the 20th century, including an increase of surface air temperature (Moritz et al., 2002; D'Andrea et al., 2012). In the future, further changes in sea ice coverage, glacier dynamics, wind speeds and directions, and primary production are expected (e.g., Loeng et al., 2005; Denman et al., 2007; Radić and Hock, 2011; Slagstad et al., 2011). Svalbard glaciers have retreated significantly in the past 50 years (Dowdeswell, 1995; Nordli et al., 1996; Ziaja, 2001), which has resulted in increased supply of terrigenous, glacially derived material to several fjords (e.g., Elverhøi et al., 1995; Zajączkowski et al., 2004). This effect is predicted to continue over future decades (Syvitski and Andrews, 1994; Syvitski, 2002; Trusel et al., 2010). The three fjords investigated in our study may portray different stages in the development of fjord environments affected by glacier retreat and sediment delivery. Kongsfjorden and Van Keulenfjorden are characterized by large tidewater glaciers partially experiencing post-surge quiescent-phase conditions (Trusel et al., 2010) and high meltwater and

sediment delivery rates (Syvitski, 2002; Trusel et al., 2010). In contrast, Smeerenburgfjorden has experienced strong retreat of its main glacier, Smeerenburgbreen (Velle, 2012), and, due to the relatively small remaining glacial drainage area (Blaszczyk et al., 2009), is likely affected by smaller sediment input. The following implications regarding the development of biogeochemical processes in Arctic fjords, such as those of Svalbard, can be deduced from our study:

(1) As a result of the increased glacial runoff, it is likely that biogeochemical processes within tidewater glacier-influenced fjords during initial stages of glacier retreat and increased sediment delivery will more closely resemble the setting described for Van Keulenfjorden and Kongsfjorden (Figs. 9 and 10). These fjords are characterized by high iron delivery due to enhanced meltwater runoff from adjacent glaciers; this process is a key driver of carbon mineralization during DIR in the fjord sediments. As a consequence of the high concentration of porewater dissolved iron, there is a continued flux of diagenetically recycled iron from the porewater into the water column. The recurring benthic recycling-transport mechanism contributes to the oxic transfer of glacially derived iron outward to the continental shelf. With the development of water column stratification in spring and summer, fine-grained, Fe_{HR}-enriched particulate iron contained within the surface meltwater plume may be transported seaward. The input of iron originating directly from glacial sources and benthic iron recycling may help sustain primary production in the highly productive waters of the western Svalbard continental shelf (Sakshaug, 2004; Reigstad et al., 2011). This area is characterized by high accumulation rates of organic carbon and is proposed to be an important sink for carbon dioxide (Winkelmann and Knies, 2005). In other Arctic shelf waters where primary productivity is suppressed by sea ice coverage, and where salinity stratification exerts a strong control on nutrient supply (Carmack and Wassmann, 2006), future sea-ice retreat and enhanced glacial iron supply may support increases in production (Lalande et al., 2009; Popova et al., 2010; Slagstad et al., 2011).

(2) With further glacial retreat, the long-term changes to the fjord environment may negatively impact the delivery of glacial iron to the outer shelf. The development of large proglacial zones does not necessarily reduce the input of fine-grained, easily reducible iron phases to the adjacent fjords. Shrinking glaciers and associated decreasing glacial runoff may, however, limit the overall rate of sediment delivery and result in lower metal accumulation in fjord sediments (Figs. 9 and 10). These factors will likely contribute to a reduction of the amount of dissolved and particulate iron being delivered from glaciated areas to the adjacent continental shelves. At the same time, higher primary productivity, facilitated by enhanced light penetration in the fjords, will lead to increased input of marine organic matter to the sediment and promote elevated organic carbon remineralization. Dissolved iron and sulfide-reactive iron oxide phases will become depleted in the surface sediments due to elevated organoclastic sulfate reduction rates, as observed for Smeerenburgfjorden. Importantly, the dominance of sulfate-reducing conditions in the sediments will limit benthic iron recycling in these fjords and increase the efficiency of iron entrapment as iron sulfides in the sediment (Fig. 9). The combination of these processes will reduce the amount of recycled iron in the water column available for transport to the outer shelf. Together with the diminished runoff of fine-grained Fe_{HR} in a smaller meltwater plume, the net result could be a reduced delivery of glacially derived iron to high-latitude continental margins in the future as more fjords become subject to pronounced glacial retreat. An important factor remains the production of organic matter in the fjords and its dilution in the sediment, which will determine the rate of carbon mineralization and influence the participation of the different terminal electron-accepting processes in the overall oxidation of organic carbon (Fig. 9).

6. SUMMARY AND CONCLUSIONS

Our results indicate that high-latitude fjords are dynamic biogeochemical environments strongly influenced by the behavior of local glaciers. Glacial sediments can exhibit a wide range of iron compositions, likely controlled by glacier bedrock mineralogy and hydrodynamic processes within and beneath adjacent glaciers, and size-sorting of the meltwater particulate phase during passage across the proglacial zones. Extreme sedimentation rates in the fjords lead to very high iron accumulation rates accompanied by comparably low organic carbon input and dilution in the sediment, particularly in Kongsfjorden and Van Keulenfjorden. Importantly, these factors enable a prominent role of glacially derived iron as the key driver for biogeochemical processes in the fjord sediments. We propose a recurring pattern of iron deposition-recycling, facilitating an increased flux of dissolved iron produced during dissimilatory metal reduction to the water column and subsequent re-oxidation to “fresh” and likely nanoparticulate iron. This rejuvenating mechanism, along with the distinct oceanographic characteristics of fjords, may ultimately lead to the delivery of glacially derived iron to the adjacent shelf where it may support primary productivity in the surface waters. Importantly, this oxic transport mechanism for glacially derived iron has not previously been considered in estimates and models for the iron flux from glacial fjords to the continental shelf. In the glaciated fjords of Svalbard, the high Fe_{HR} delivery rate may be a key factor that promotes the occurrence of DIR and ultimately the flux of iron to the water column. Our results from the western Svalbard fjords thus provide support for the recently emerging picture (Severmann et al., 2010; Homoky et al., 2013) that the weathering regime and hydro-climatic factors on land, which control the solid-phase iron supply to continental margin sediments, are key factors that determine the ben-

thic dissolved iron flux to the overlying seawater. Further studies are needed to decipher the cycling and bioavailability of iron phases in the water column of the Svalbard fjords and shelf, and more generally in the different Arctic shelf regions. Our study supports the hypotheses by Macdonald and Gobeil (2012) and März et al. (2011, 2012) for an efficient shuttle for glacially derived iron and manganese from high latitude coastal and shelf environments to the deep ocean basins, such as the Central Arctic Ocean, during interglacials.

ACKNOWLEDGMENTS

The 2010 and 2011 sampling campaigns were funded by the Max Planck Institute for Marine Microbiology (MPI-MM), Bremen. We would like to thank B.B. Jørgensen and M.M.M. Kuypers for their support of this study. The captains and crews of the 2010 and 2011 sampling campaigns along with all of the members of the 2010 and 2011 Svalbard scientific parties are thanked for their assistance aboard R/V *Farm* and during lab work in Ny Ålesund. We also thank the staff of the Kings Bay Marine Laboratory and the AWIPEV Arctic Research Base for their great support. A. Schipper, K. Imhoff, T. Max and B. Brunner provided help during laboratory work at the MPI-MM, Bremen. We thank S. Bates for assistance with sulfur isotope analyses at UC Riverside and C. Gott and E. Goldbaum for assistance with iron analyses. C. März is thanked for helpful comments on an earlier version of the manuscript. L.M. Wehrmann acknowledges funding by a German Research Foundation (DFG) research fellowship (We 5015/1-1 and /2-1) for this study and N. Riedinger was supported by the U.S. NASA Postdoctoral Program. The U.S. NSF provided additional funds (N.R., T.W.L.). We would like to thank three anonymous reviewers and the AE S. Severmann for their insightful comments and advice that helped improving this manuscript.

APPENDIX A. SUPPLEMENTARY DATA

Supplementary data associated with this article can be found, in the online version, at http://dx.doi.org/10.1016/j.gca.2014.06.007.

REFERENCES

Ahke A. (2007) Composition of molecular organic matter pools, pigments and proteins. In *Benguela upwelling and Arctic Sediments*. Berichte, Fachbereich Geowissenschaften, No. **256**. Springer, p. 200.

Aller R. C. (1994) The sedimentary Mn cycle in Long Island Sound: its role as intermediate oxidant and the influence of bioturbation, O_2, and Corg flux on diagenetic reaction balances. *J. Mar. Res.* **52**, 259–295.

Aller R. C., Mackin J. E. and Cox, Jr., R. T. (1986) Diagenesis of Fe and S in Amazon inner shelf muds: apparent dominance of Fe reduction and implications for the genesis of ironstones. *Con. Shelf Res.* **6**, 263–289.

Aller R. C. and Aller J. Y. (1998) The effect of biogenic irrigation intensity and solute exchange on diagenetic reaction rates in marine sediments. *J. Mar. Res.* **56**, 905–936.

Alongi D. M. (1995) Decomposition and recycling of organic matter in muds of the Gulf of Papua, northern Coral Sea. *Con. Shelf Res.* **15**, 1319–1337.

Anisimov O. A., Vaughan D. G., Callaghan T. V., Furgal C., Marchant H. and Prowse T. D., et al. (2007) Polar regions (Arctic and Antarctic). In *Climate Change 2007: Impacts, Adaptation and Vulerability. Contribution of Working Group II to the Forth Assessment Report of the Intergovernmental Panel on Climate Change* (eds. M. L. Parry, O. F. Canziani, J. P. Palutikof, P. J. van der Linden and C. E. Hanson). Cambridge University Press, Cambridge, pp. 653–685.

Arrigo K. R., van Dijken G. L. and Pabi S. (2008) Impact of a shrinking Arctic ice cover on marine primary production. *Geophys. Res. Lett.* **35**, L19606. http://dx.doi.org/10.1029/2008GL035028.

Barbeau K., Moffett J. W., Caron D. A., Croot P. L. and Erdner D. L. (1996) Role of protozoan grazing in relieving iron limitation of phytoplankton. *Nature* **380**, 61–64.

Barbeau K., Rue E. L., Bruland K. W. and Butler A. (2001) Photochemical cycling of iron in the surface ocean mediated by microbial iron(III)-binding ligands. *Nature* **413**, 409–413.

Berner R. A. (1970) Sedimentary pyrite formation. *Am. J. Sci.* **268**, 1–23.

Berner R. A. and Raiswell R. (1984) C/S method for distinguishing fresh-water from marine sedimentary rocks. *Geology* **12**, 365–368.

Berg P., Risgaard-Petersen N. and Rysgaard S. (1998) Interpretation of measured concentration profiles in sediment pore water. *Limnol. Oceanogr.* **43**, 1500–1510.

Berg P., Rysgaard S. and Thamdrup B. (2003) Dynamic modeling of early diagenesis and nutrient cycling. A case study in an Arctic marine sediment. *Am. J. Sci.* **303**, 509–555.

Bhatia M. P., Kujawinski E. B., Das S. B., Breier C. F., Henderson P. B. and Charette M. A. (2013) Greenland meltwater as a significant and potentially bioavailable source of iron to the ocean. *Nat. Geosci.* **6**, 274–278.

Blaszczyk M., Jania J. A. and Hagen J. O. (2009) Tidewater glaciers of Svalbard: Recent changes and estimates of calving fluxes. *Polish Polar Res.* **30**(2), 85–182.

Blatt H., Tracy R. and Owens B. (2005) *Petrology: Igneous, Sedimentary, and Metamorphic*, third ed. W. H. Freeman, p. 530.

Bligh M. W. and Waite D. (2011) Formation, reactivity, and aging of ferric oxide particles formed from Fe(II) and Fe(III) sources: Implications for iron bioavailability in the marine environment. *Geochim. Cosmochim. Acta* **75**, 7741–7758.

Borer P. M., Sulzberger B., Reichard P. and Kraemer S. P. (2005) Effect of siderophores on the light-induced dissolution of colloidal iron(III) (hydr)oxides. *Mar. Chem.* **93**, 179–193.

Boudreau B. P. (1997) *Diagenetic Models and Their Implementation: Modelling Transport and Reaction in Aquatic Sediments*. Springer-Verlag, Berlin, p. 414.

Boudreau B. P. and Scott M. R. (1978) A model for the diffusion-controlled growth of deep-sea manganese nodules. *Am. J. Sci.* **278**, 903–929.

Boyé M., Nishioka J., Croot P., Laan P., Timmermans K. R., Strass V. H., Takeda S. and de Baar H. J. W. (2010) Significant portion of dissolved organic Fe complexes in fact is Fe colloids. *Mar. Chem.* **122**, 20–27.

Boyd P. W., Watson A. J., Law C. S., Abraham E. R., Trull T., Murdoch R., Bakker D. C. E., Bowie A., Buesseler K. O., Chang H., Charett M., Croot P., Downing K., Frew R., Gall M., Hadfield M., Hall J., Harvey M., Jameson G., LaRoche J., Liddicoat M., Ling R., Maldonado M. T., McKay R. M., Nodder S., Pickmere S., Pridmore R., Rintoul S., Safi K., Sutton P., Strzepek R., Tanneberger K., Turner S., Waite A. and Zeldis J. (2000) A mesoscale phytoplankton bloom in the polar Southern Ocean stimulated by iron fertilization. *Nature* **407**, 695–702.

Boyd P. W. and Ellwood M. J. (2010) The biogeochemical cycle of iron in the ocean. *Nat. Geosci.* **3**, 672–682. http://dx.doi.org/10.1038/NGEO964.

Breitbarth E., Achterberg E. P., Ardelan M. V., Baker A. R., Bucciarelli E., Chever F., Croot P. L., Duggen S., Gledhill M., Hassellöv M., Hassler C., Hoffmann L. J., Hunter K. A., Hutchins D. A., Ingri J., Jickells T., Lohan M. C., Nielsdóttir M. C., Sarthou G., Schoemann V., Trapp J. M., Turner D. R. and Ye Y. (2010) Iron biogeochemistry across marine systems-progress from the past decade. *Biogeoscience* **7**, 1075–1097.

Brown G. H. (2002) Review: Glacier meltwater hydrochemistry. *Appl. Geochem.* **17**, 855–883.

Brüchert V., Knoblauch C. and Jørgensen B. B. (2001) Controls on stable sulfur isotope fractionation during bacterial sulfate reduction in Arctic sediments. *Geochim. Cosmochim. Acta* **65**, 763–776.

Bruland K. W., Orians K. J. and Cowen J. P. (1994) Reactive trace metals in the stratified central North Pacific. *Geochim. Cosmochim. Acta* **58**, 3171–3182.

Burdige D. J. and Nealson K. H. (1986) Chemical and microbial studies of sulfide-mediated manganese reduction. *Geomicrobiol J.* **4**, 361–387.

Burdige D. J. (1993) The biogeochemistry of manganese and iron reduction in marine sediments. *Earth-Sci. Rev.* **35**, 249–284.

Canfield D. E., Jørgensen B. B., Fossing H., Glud R., Gundersen J., Ramsing N. B., Thamdrup B., Hansen J. W., Nielsen L. P. and Hall P. O. J. (1993a) Pathways of organic carbon oxidation in three continental margin sediments. *Mar. Geol.* **113**, 27–40.

Canfield D. E., Thamdrup B. and Hansen J. W. (1993b) The anaerobic degradation of organic matter in Danish coastal sediments – Iron reduction, manganese reduction, and sulfate reduction. *Geochim. Cosmochim. Acta* **57**, 3867–3883.

Carmack E. and Wassmann P. (2006) Food webs and physicalbiological coupling on pan-Arctic shelves: unifying concepts and comprehensive perspectives. *Prog. Oceanogr.* **71**, 446–477. http://dx.doi.org/10.1016/j.pocean.2006.10.004.

Carmack E., Barber D., Christensen J. H., Macdonald R., Rudels B. and Sakshaug E. (2006) Climate variability and physical forcing of the food webs and the carbon budget on panarctic shelves. *Prog. Oceanogr.* **72**, 145–181. http://dx.doi.org/10.1016/j.pocean.2006.10.005.

Chen M. and Wang W. X. (2001) Bioavailability of natural colloidal Fe to marine plankton: influence of colloidal size and aging. *Limnol. Oceanogr.* **46**, 1956–1967.

Chen M., Dei R. C. H., Wang W.-X. and Guo L. (2003) Marine diatom uptake of iron bound with natural colloids of different origins. *Mar. Chem.* **81**, 177–189.

Cline J. D. (1969) Spectrophotometric determination of hydrogen sulfide in natural waters. *Limnol. Oceanogr.* **14**, 454–458.

Coale K. H. (1991) The effects of iron, manganese, copper and zinc on primary production and biomass in plankton of the Subarctic Pacific. *Limnol. Oceanogr.* **36**, 1851–1864.

Coale K. H., Johnson K. S., Fitzwater S. E., Gordon R. M., Tanner S., Chavez F. P., Ferioli L., Sakamoto C., Rogers P., Millero F., Steinberg P., Nightingale P., Cooper D., Cochlan W. P., Landry M. R., Constantinou J., Rollwagen G., Trasvina A. and Kudela R. (1996) A massive phytoplankton bloom induced by an ecosystem-scale iron fertilization experiment in the equatorial Pacific Ocean. *Nature* **383**, 495–501.

Cooper R. J., Wadham J. L., Tranter M., Hodgkins R. and Peters N. E. (2002) Groundwater hydrochemistry in the active layer of the proglacial zone, Finsterwalderbreen, Svalbard. *J. Hydrol.* **269**, 208–223.

Comiso J. C., Parkinson C. L., Gersten R. and Stock L. (2008) Accelerated decline in the Arctic sea ice cover. *Geophys. Res. Lett.* **35**, L01703.

Cottier F., Tverberg V., Inall M., Svendsen H., Nilsen F. and Griffiths C. (2005) Water mass midofication in an Arctic fjord through cross-shelf exchange: the seasonal hydrography of Kongsfjorden, Svalbard. *J. Geophys. Res.* **110**, C12005.

Cottier F. R., Nilsen F., Skogseth R., Tverberg V., Skardhamar J. and Svendsen H. (2010) Arctic fjords: a review of the oceanographic environment and dominant physical processes. In *Fjord Systems and Archives. Geological Society* (eds. J. A. Howe, W. E. N. Austin, M. Forwick and M. Paetzel). Special Publications, London, Vol. 344, pp. 35–50.

Cowan E. A. and Powell R.D. (1990) Suspended sediment transport and deposition of cyclically interlaminated sediment in a temperate glacial fjord, Alaska, U.S.A. In *Glacimarine Environments: Processes and Sediments, vol. 53* (eds. J. A. Dowdeswell and J. D. Scourse). Geol. Soc. Spec. Publ. pp. 75–89.

Cowan E. A. and Powell R. D. (1991) Ice-proximal sediment accumulation rates in a temperate glacial fjord, southeastern Alaska. In *Glacial Marine Sedimentation: Paleoclimatic Significance* (eds. J. Anderson and G. M. Ashley). Spec. Pap. Geol. Soc. Am. **261**. pp. 61–73.

Cullen J. T., Bergquist B. A. and Moffett J. W. (2006) Thermodynamic characterization of the partitioning of iron between soluble and colloidal species in the Atlantic Ocean. *Mar. Chem.* **98**, 295–303.

D'Andrea W. J., Vaillencourt D. A., Balascio N. L., Werner A., Roof S. R., Retelle M. and Bradley R. S. (2012) Mild Little Ice Age and unprecedented recent warmth in an 1800 year lake sediment record from Svalbard. *Geology* **40**, 1007–1010.

Dallmann W. K., Hjelle A., Ohta Y., Salvigsen O., Bjornerud M. G., Hauser E. C., Maher H. D. and Craddock C. (1990) *Geological Map, Svalbard.* Van Keulenfjorden B11G, Norsk Polarinstitutt, Oslo.

Dallmann W. K., Ohta Y., Elvevold S. and Blomeier D. (2002) *Bedrock Map of Svalbard and Jan Mayen*. Norsk Polarinstitutt Temakart No. 33, Norsk Polarinstitutt, Oslo.

de Baar H. J. W. and de Jong J. T. M. (2001) Distributions, sources and sinks of iron in seawater. In *Biogeochemistry of Iron in Seawater* (eds. D. Turner and K. A. Hunter). IUPAC Book Series on Analytical and Physical Chemistry of Environmental Systems **7**, 123–253.

de Jong J., Schoemann V., Lannuzel D., Croot P., de Baar H. and Tison J. L. (2012) Natural iron fertilization of the Atlantic Southern Ocean by continental shelf sources of the Antarctic Peninsula. *J. Geophys. Res.* **117**, G01029.

de Jong J. T. M., Schoemann V., Maricq N., Mattielli N., Langhorne P., Haskell T. and Tison J.-L. (2013) Iron in landfast sea ice of McMurdo Sound derived from sediment resuspension and wind-blown dust attributes to primary productivity in the Ross Sea, Antarctica. *Mar. Chem.* **157**, 24–40.

Denman K. L., Brasseur G., Chidthaisong A., Ciais P., Cox P. M., Dickinson R. E., Hauglustaine D., Heinze C., Holland E., Jacob D., Lohman U., Ramachandran S., da Silva Dias P. L., Wofsy S. C. and Zhang X. (2007) Coupling between changes in the climate system and biogeochemistry. In *Climate Change 2007: The Physical Science Basis. Contribution of Working Group I to the Fourth Assessment Report of the Intergovernmental Panel on Climate Change* (eds. S. Solomon, D. Qin, M. Manning, Z. Chen, M. Marquis, K. B. Averyt, M. Tignor and H. L. Miller). Cambridge University Press, Cambridge, pp. 512–533.

Dickens G. R., Kölling M., Smith D. C. and Schnieders L. (2007) Rhizon sampling of pore waters on scientific drilling expeditions: an example from the IODP expedition 302, Arctic Coring Expedition (ACEX). *Sci. Drilling* **4**, 22–25.

Dowdeswell J. A. and Cromack M. (1991) Behavior of a glacier-derived suspended sediment plume in a small Arctic inlet. *J. Geol.* **99**, 111–123.

Dowdeswell J. A. (1995) Glaciers in the High Arctic and recent environmental change. *Philos. Trans. R. Soc. London* **A352**, 321–334.

Elrod V. A., Berelson W. M., Coale K. H. and Johnson K. S. (2004) The flux of iron from continental shelf sediments: a missing source for global budgets. *J. Geophys. Res.* **31**, L12307.

Elverhøi A., Svendsen J. I., Solheim A., Andersen E. S., Milliman J., Mangerud J. and Hooke R. L. (1995) Late Quaternary sediment yield from the high Arctic Svalbard area. *J. Geol.* **103**, 1–17.

Falkowski P. G. (1997) Evolution of the nitrogen cycle and its influence on the biological sequestration of CO_2 in the ocean. *Nature* **387**, 272–275.

Falkowski P. G., Barber R. T. and Smetacek V. (1998) Biogeochemical controls and feedbacks on ocean primary production. *Science* **281**, 200–206.

Feijtel T. C., DeLaune R. D. and Patrick, Jr., W. H. (1988) Biogeochemical control on metal distribution and accumulation in louisiana sediments. *J. Environ. Qual.* **17**(1), 88–94.

Fossing H. and Jørgensen B. B. (1989) Measurement of bacterial sulfate reduction in sediments – evaluation of a single-step chromium reduction method. *Biogeochemistry* **8**, 205–222.

Froelich P. N., Klinkhammer G. P., Bender M. L., Luedtke N. A., Heath G. R., Cullen D., Dauphin P., Hammond D., Hartman B. and Maynard V. (1979) Early oxidation of organic matter in pelagic sediments of the eastern equatorial Atlantic: suboxic diagenesis. *Geochim. Cosmochim. Acta* **43**, 1075–1090.

Gaidos E., Lanoil B., Thorsteinsson T., Graham A., Skidmore M., Han S.-K., Rust T. and Popp B. (2004) A viable microbial community in a subglacial volcanic crater lake, Iceland. *Astrobiology* **4**, 327–344.

Gerringa L. J. A., Alderkamp A.-C., Laan P., Thuróczy C.-E., De Baar H. J. W., Mills M. M., van Dijken G. L., van Haren H. and Arrigo K. R. (2012) Iron from melting glaciers fuels the phytoplankton blooms in Amundsen Sea (Southern Ocean): Iron biogeochemistry. *Deep Sea Res.* **71–76**, 16–31.

Giles K. A., Laxon S. W. and Ridout A. L. (2008) Circumpolar thinning of Arctic sea ice following the 2007 record ice extent minimum. *Geophys. Res. Lett.* **35**(22), L22502. http://dx.doi.org/10.1029/2008GL035710.

Glasser N. F. and Hambrey M. J. (2001) Styles of sedimentation beneath Svalbard valley glaciers under changing dynamic and thermal regimes. *J. Geol. Soc. London* **158**, 697–707.

Gledhill M. and Buck K. N. (2012) The organic complexation of iron in the marine environment: a review. *Front. Microbiol.* **3**, 1–17.

Glud R. N., Holby O., Hoffmann F. and Canfield D. E. (1998) Benthic mineralization and exchange in Arctic sediments (Svalbard, Norway). *Mar. Ecol. Prog. Ser.* **173**, 237–251.

Gobeil C., Macdonald R. W. and Sundby B. (1997) Diagenetic separation of cadmium and manganese in suboxic continental margin sediments. *Geochim. Cosmochim. Acta* **61**, 4647–4654.

Hagen J. O., Liestøl O., Roland E. and Jørgensen T. (1993) *Glacier Atlas of Svalbard and Jan Mayen*. Norsk Polarinstitutt Meddelser, 129.

Harland W. B. (1997) The Geology of Svalbard. The Geological Society, Bath. *Geol. Soc. Memoir* **17**, 529.

Hassler C. S. and Schoemann V. (2009) Bioavailability of organically bound Fe to model phytoplankton of the Southern Ocean. *Biogeosciences* **6**, 2281–2296.

Hassler C. S., Schoemann V., Nichols C. M., Butler E. C. V. and Boyd P. W. (2011) Saccharides enhance iron bioavailability to Southern Ocean phytoplankton. *PNAS* **108**, 1076–1081.

Hawkings J. R., Wadham J. L., Tranter M., Raiswell R., Benning L. G., Statham P. J., Tedstone A., Nienow P., Lee K. and Telling J. (2014) Ice sheets as a significant source of highly reactive nanoparticulate iron to the oceans. *Nat. Comm.* **5**. http://dx.doi.org/10.1038/ncomms4929.

Hjelle A. (1993) The geology of Svalbard: Oslo, Polarhåndbok no. 6, Norsk Polarinstitutt, pp. 163.

Hebbeln D. and Berner H. (1993) Surface sediment distribution in the Fram Strait. *Deep Sea Res. Part I* **40**, 1731–1745.

Heggie D., Klinkhammer G. and Cullen D. (1987) Manganese and copper fluxes from continental margin sediments. *Geochim. Cosmochim. Acta* **51**, 1059–1070.

Hodgkins R. (1997) Glacier Hydrology in Svalbard, Norwegian High Arctic. *Quat. Sci. Rev.* **16**, 957–973.

Hodgkins R., Cooper R., Wadham J. and Tranter M. (2003) Suspended sediment fluxes in a high-Arctic glacierised catchment: implications for fluvial sediment storage. *Sed. Geol.* **162**, 105–117.

Hodgkins R., Cooper R., Wadham J. and Tranter M. (2009) The hydrology of the proglacial zone of a high-Arctic glacier (Finsterwalderbreen, Svalbard): atmospheric and surface water fluxes. *J. Hydrol.* **378**, 150–160.

Hodson A. J. and Ferguson R. I. (1999) Fluvial suspended sediment transport from cold and warm-based glaciers in Svalbard. *Earth Surf. Proc. Landforms* **24**, 957–974.

Hölemann J. A., Schirmacher M. and Prange A. (2005) Seasonal variability of trace metals in the Lena River and the southeastern Laptev Sea: impact of the spring freshnet. *Global Planet. Change* **48**, 112–125.

Holte B., Dahle S., Gulliksen B. and Næs K. (1996) Some macrofaunal effects of local pollution and glacier-induced sedimentation, with indicative chemical analyses, in the sediments of two Arctic fjords. *Polar Biol.* **16**, 549–557.

Homoky W. B., Severmann S., McManus J., Berelson W. M., Riedel T. E., Statham P. J. and Mills R. A. (2012) Dissolved oxygen and suspended particles regulate the benthic flux of iron from continental margins. *Mar. Chem.* **134–135**, 59–70.

Homoky W. B., John S. G., Conway T. M. and Mills R. A. (2013) Distinct iron isotopic signatures and supply from marine sediment dissolution. *Nat. Commun.* **4**, 2143.

Hop H., Pearson T., Hegseth E. N., Kovacs K. M., Wiencke C., Kwasniewski S., Eiane K., Mehlum F., Gulliksen B., Wlodarska-Kowalczuk M., Lydersen C., Weslawski J. M., Cochrane S., Gabrielsen G. W., Leakey R. J. G., Lønne O. J., Zajaczkowski M., Falk-Petersen S., Kendall M., Wängberg S.-Å., Bischof K., Voronkov A. Y., Kovaltchouk N. A., Wiktor J., Poltermann M., di Prisco G., Papucci C. and Gerland S. (2002) The marine ecosystem of Kongsfjorden, Svalbard. *Polar Res.* **21**, 167–208.

Howe J. A., Moreton S. G., Morri C. and Morris P. (2003) Multibeam bathymetry and the depositional environments of Kongsfjorden and Krossfjorden, western Spitsbergen, Svalbard. *Polar Res.* **22**, 301–316.

Howe J. A., Austin W. E. N., Forwick M., Paetzel M., Harland R. and Cage A. G. (2010) Fjord systems and archives: a review. In *Fjord Systems and Archives. Geological Society* (eds. J. A. Howe, W. E. N. Austin, M. Forwick and M. Paetzel). Special Publications, London, pp. 5–15, 344, doi: 10.1144/SP344.2.

Hubert C., Loy A., Nickel M., Arnosti C., Baranyi C., Brüchert V., Ferdelman T., Finster K., Christensen F. M., Rezende J. R., Vandieken V. and Jørgensen B. B. (2009) A constant flux of diverse thermophilic bacteria into the cold arctic seabed. *Science* **325**(5947), 1541–1544.

Hunter K. A. and Boyd P. W. (2007) Iron-binding ligands and their role in the ocean biogeochemistry of iron. *Environ. Chem.* **4**, 221–232.

Hurst M. P., Aguilar-Islas A. M. and Bruland K. (2010) Iron in the southeastern Bering Sea: elevated leachable particulate Fe in shelf bottom waters as an important source for surface waters. *Cont. Shelf Res.* **30**, 467–480.

Hutchins D. A. and Bruland K. W. (1998) Iron-limited diatom growth and Si:N uptake ratios in a coastal upwelling regime. *Nature* **393**, 561–564.

Hutchins D. A., Witter A. E., Butler A. and Luther, III, G. W. (1999) Competition among marine phytoplankton for different chelated iron species. *Nature* **400**, 858–861.

Jensen M. M., Thamdrup B., Rysgaard S., Holmer M. and Fossing H. (2003) Rates and regulation of microbial iron reduction in sediments of the Baltic-North Sea transition. *Biogeochemistry* **65**, 297–317.

Jickells T. D. and Spokes L. J. (2001) Atmospheric iron inputs to the oceans. In *The Biogeochemistry of Iron in Seawater* (eds. D. R. Turner and K. A. Hunter). John Wiley, Hoboken, NJ, pp. 85–118.

Jickells T. D., An Z. S., Andersen K. K., Baker A. R., Bergametti G., Brooks N., Cao J. J., Boyd P. W., Duce R. A., Hunter K. A., Kawahata H., Kubilay N., laRoche J., Liss P. S., Mahowald N., Prospero J. M., Ridgwell A. J., Tegen I. and Torres R. (2005) Global Iron Connections Between Desert Dust, Ocean Biogeochemistry, and Climate. *Science* **308**, 67–71.

Johnson K. S., Berelson W. M., Coale K. H., Coley T. L., Elrod V. A., Fairey W. R., Iams H. D., Kilgore T. E. and Nowicki J. L. (1992) Manganese flux from continental margin sediments in a transect through the oxygen minimum. *Science* **257**, 1242–1245.

Johnson K. S., Chavez F. P. and Friederich G. E. (1999) Continental-shelf sediment as a primary source of iron for coastal phytoplankton. *Nature* **398**, 697–700.

Jørgensen B. B., Glud R. N. and Holby O. (2005) Oxygen distribution and bioirrigation in Arctic fjord sediments (Svalbard, Barents Sea). *Mar. Ecol. Prog. Ser.* **295**, 85–95.

Jørgensen B. B. and Kasten S. (2006) Sulfur cycling and methane oxidation. In: *Marine Geochemistry* (eds. H.D. Schulz and M. Zabel). Springer–Verlag, Heidelberg. p. 574.

Kamyshny, Jr., A. and Ferdelman T. G. (2010) Dynamics of zero-valent sulfur species including polysulfides at seep sites on intertidal sand flats (Wadden Sea, North Sea). *Mar. Chem.* **121**(1–2), 17–26.

Kanneworff E. and Nicolaisen W. (1983) A simple, hand-operated quantitative bottom sampler. *Ophelia* **22**(2), 253–255.

Kempf P., Forwick M., Laberg J. S. and Vorren T. O. (2013) Late Weichselian and Holocene sedimentary palaeoenvironment and glacial activity in the high-arctic van Keulenfjorden, Spitsbergen. *The Holocene* **23**(11), 1607–1618.

Knauer G. A., Martin J. H. and Gordon R. M. (1982) Cobalt in north-east Pacific waters. *Nature* **297**, 49–51.

Krachler R., Jirsa F. and Ayromlou S. (2005) Factors influencing the dissolved iron input by river water to the open ocean. *Biogeosciences* **2**, 311–315.

Kraemer S. M. (2004) Iron oxide dissolution and solubility in the presence of siderophores. *Aquat. Sci.* **66**, 3–18.

Kranck K. (1973) Flocculation of suspended sediment in the sea. *Nature* **246**(5432), 348–350.

Kohler J., James T. D., Murray T., Nuth C., Brandt O., Barrand N. E., Aas H. F. and Luckman A. (2007) Acceleration in thinning rate on western Svalbard glaciers. *Geophys. Res. Lett.* **34**, L18502.

Kostka J. E., Thamdrup B., Glud R. N. and Canfield D. (1999) Rates and pathways of carbon oxdation in permanently cold Arctic sediments. *Mar. Ecol. Prog. Series* **180**, 7–21.

Lalande C., Belanger S. and Fortier L. (2009) Impact of a decreasing sea ice cover on the vertical export of particulate organic carbon in the northern Laptev Sea, Siberian Arctic Ocean. *Geophys. Res. Lett.* **36**, L21604. http://dx.doi.org/10.1029/2009GL040570.

Lam P. J. and Bishop J. K. B. (2008) The continental margin is a key source of iron to the HNLC North Pacific Ocean. *Geophys. Res. Lett.* **35**, L07608.

Lannuzel D., Schoemann V., de Jong J., Tison J. L. and Chou L. (2007) Distribution and biogeochemical behaviour of iron in the East Antarctic sea ice. *Mar. Chem.* **106**, 18–32.

Lannuzel D., Schoemann V., de Jong J., Chou L., Delille B., Becquevort S. and Tison J.-L. (2008) Iron study during a time series in the western Weddell pack ice. *Mar. Chem.* **108**, 85–95.

Lannuzel D., Schoemann V., de Jong J., Pasquer B., van der Merwe P., Masson F., Tison J.-L. and Bowie A. (2010) Distribution of dissolved iron in Antarctic sea ice. Spatial, seasonal, and inter-annual variability. *J. Geophys. Res.* **115**, G03022.

Lannuzel D., van der Merwe P. C., Townsend A. T. and Bowie A. R. (2014) Size fractionation of iron, manganese and aluminium in Antarctic fast ice reveals a lithogenic origin and low iron solubility. *Mar. Chem.* **161**, 47–56.

Lanoil B., Skidmore M., Priscu J. C., Han S., Foo W., Vogel S. W., Tulaczyk S. and Engelhardt H. (2009) Bacteria beneath the West Antarctic Ice Sheet. *Environment. Microbiol.* **11**, 609–615.

Lettmann K. A., Riedinger N., Ramlau R., Knab N., Böttcher M. E., Khalili A., Wolff J.-O. and Jørgensen B. B. (2012) Estimation of biogeochemical rates from concentration profiles: a novel inverse method. *Estuar. Coast. Shelf Sci.* **100**, 26–37.

Lin H., Rauschenberg S., Hexel C. R., Shaw T. J. and Twining B. S. (2011) Free-drifting icebergs as sources of iron to the Weddell Sea. *Deep-Sea Res. II* **58**, 1392–1406.

Lippiatt S. M., Lohan M. C. and Bruland K. W. (2010) The distribution of reactive iron in northern Gulf of Alaska coastal waters. *Mar. Chem.* **121**, 187–199.

Loeng H., Brander K., Carmack E., Denisenko S., Drinkwater K., Hansen B., Kovacs K., Livingston P., McLaughlin F. and Sakshaug E. (2005) Marine Systems. In *Arctic Climate Impact Assessment – Scientific Report*. Cambridge University Press, Cambridge, pp. 453–538.

Lovley D. R. (1991) Dissimilatory Fe(III) and Mn(IV) reduction. *Microbiol. Rev.* **55**, 259–287.

Lovley D. R. (1997) Microbial Fe(III) reduction in subsurface environments. *FEMS Microbiol. Rev.* **20**, 305–313.

Lyle M. W. and Dymond J. (1976) Metal accumulation rates in the southeast pacific — errors introduced from assumed bulk densities. *Earth Planet. Sci. Lett.* **30**, 164–168.

Lyons T. W. and Severmann S. (2006) A critical look at iron paleoredox proxies: new insights from modern euxinic marine basins. *Geochim. Cosmochim. Acta* **70**, 5698–5722.

Macdonald R. W. and Gobeil C. (2012) Manganese sources and sinks in the Arctic Ocean with reference to periodic enrichments in basin sediments. *Aquat. Geochem.* **18**(6), 565–591.

Maldonado M. T. and Price N. M. (2001) Reduction and transport of organically bound iron by *Thalassiosira oceanica* (Bacillariophyceae). *J. Phycol.* **37**, 298–309.

Maldonado M. T., Allen A. E., Chong J. S., Lin K., Leus D., Karpenko N. and Harris S. L. (2006) Copper-dependent iron transport in coastal and oceanic diatoms. *Limnol. Oceanogr.* **51**(4), 1729–1743.

Martin J. H. and Fitzwater S. E. (1988) Iron deficiency limits phytoplankton growth in the north-east Pacific subarctic. *Nature* **331**, 341–343.

Martin J. H. (1990) Glacial-interglacial CO_2 change: the iron hypothesis. *Paleoceanography* **5**(1), 1–13.

Manley T. O. (1995) Branching of the Atlantic Water within the Greenland-Spitsbergen Passage: an estimate of recirculation. *J. Geophys. Res.* **100**(C10), 20,627–20,634.

März C., Stratmann A., Matthiessen J., Meinhardt A.-K., Eckert S., Schnetger B., Vogt C., Stein R. and Brumsack H.-J. (2011) Manganese-rich brown layers in Arctic sediments: composition, formation mechanisms and diagenetic overprint. *Geochim. Cosmochim. Acta* **75**, 7668–7687.

März C., Poulton S. W., Brumsack H.-J. and Wagner T. (2012) Climate-controlled variability of iron deposition in the Central Arctic Ocean (southern Mendeleev Ridge) over the last 130,000 years. *Chem. Geol.* **330–331**, 116–126.

McManus J., Berelson W. M., Severmann S., Johnson K. S., Hammond D. E., Roy M. and Coale K. H. (2012) Benthic manganese fluxes along the Oregon-California continental shelf and slope. *Cont. Shelf Res.* **43**, 71–85.

Meischner D. and Rumohr J. (1974) A light-weight, high momentum gravity corer for subaqueous sediments. *Senckenbergiana Marit.* **6**, 105–117.

Meehl G. A., Stocker T. F., Collins W. D., Friedlingstein P., Gaye A. T., Gregory J. M., Kitoh A., Knutti R., Murphy J. M., Noda A., Raper S. C. B., Watterson I. G., Weaver A. J. and Zhao Z.-C. (2007) Global Climate Projections. In *Climate Change 2007: The Physical Science Basis. Contribution of Working Group I to the Fourth Assessment Report of the Intergovernmental Panel on Climate Change* (eds. S. Solomon, D. Qin, M. Manning, Z. Chen, M. Marquis, K. B. Averyt, M. Tignor and H. L. Miller). Cambridge University Press, Cambridge, pp. 747–845.

Meredith M., Heywood K. J., Dennis P., Goldson L., White R., Fahrbach E., Schauer U. and Østerhus S. (2001) Freshwater fluxes through the western Fram Strait. *Geophys. Res. Lett.* **28**(8), 1615–1618.

Meyers P. A. (1994) Preservation of elemental an isotopic source identification of sedimentary organic matter. *Chem. Geol.* **114**, 289–302.

Middelburg J. J., Soetaert K. and Herman P. M. J. (1997) Empirical relationships for use in global diagenetic models. *Deep-Sea Res. I* **44**(2), 327–344.

Mikucki J. A., Foreman C. M., Sattler B., Lyons W. B. and Priscu J. C. (2004) Geomicrobiology of Blood Falls: an iron-rich saline discharge at the terminus of the Taylor Glacier, Antarctica. *Aquat. Geochem.* **10**(3–4), 199–220.

Millero F. J., Sotolongo S. and Izaguirre M. (1987) The oxidation kinetics of Fe(II) in seawater. *Geochim. Cosmochim. Acta* **51**, 793–801.

Millero F. J., Yao W. and Aicher J. (1995) The speciation of Fe(II) and Fe(III) in natural waters. *Mar. Chem.* **50**, 21–39.

Millero F. J. (2001) *The physical chemistry of natural waters*. Wiley-Interscience, New York.

Montross S. N., Skidmore M., Tranter M., Kivimäki A.-L. and Parkes R. J. (2012) A microbial driver of chemical weathering in glaciated systems. *Geology* **41**, 215–218.

Moore J. K. and Braucher O. (2008) Sedimentary and mineral dust sources of dissolved iron to the world ocean. *Biogeosciences* **5**, 631–656.

Morel F. M. M. and Price N. M. (2003) The biogeochemical cycles of trace metals in the oceans. *Science* **300**, 944–947.

Morgan J. J. (2005) Kinetics of reaction between O_2 and Mn(II) species in aqueous solutions. *Geochim. Cosmochim. Acta* **69**(1), 35–48.

Moritz R. E., Bitz C. M. and Steig E. J. (2002) Dynamics of recent climate change in the Arctic. *Science* **297**, 1497–1502.

Mugford R. I. and Dowdeswell J. A. (2011) Modeling glacial meltwater plume dynamics and sedimentation in high-latitude fjords. *J. Geophys. Res.* **116**, F1023. http://dx.doi.org/10.1029/2010JF001735.

Myers C. R. and Nealson K. H. (1988) Microbial reduction of manganese oxides: interactions with iron and sulfur. *Geochim. Cosmochim. Acta* **52**, 2727–2732.

Nakayama Y., Fujita S., Kuma K. and Shimada K. (2011) Iron and humic-type fluorescent dissolved organic matter in the Chukchi Sea and Canada Basin of the western Arctic Ocean. *J. Geophys. Res.* **116**, C07031.

Nealson K. H. and Myers C. R. (1992) Microbial reduction of manganese and iron: new approaches to carbon cycling. *Appl. Environ. Microbiol.* **58**, 439–443.

Nishioka J., Ono T., Saito H., Nakatsuka T., Takeda S., Yoshimura T., Suzuki K., Kuma K., Nakabayashi S., Tsumune D., Mitsudera H., Johnson W. K. and Tsuda A. (2007) Iron supply to the western subarctic Pacific: importance of iron export from the Sea of Okhotsk. *J. Geophys. Res.* **112**(C10), C10012. http://dx.doi.org/10.1029/2006JC004055.

Nilsen F., Cottier F., Skogseth R. and Mattsson S. (2008) Fjord-shelf exchanges controlled by ice and brine production: the interannual variation of Atlantic Water in Isfjorden, Svalbard. *Cont. Shelf Res.* **28**, 1838–1853. http://dx.doi.org/10.1016/j.csr.2008.04.015.

Noffke A., Hensen C., Sommer S., Scholz F., Bohlen L., Mosch T., Graco M. and Wallmann K. (2012) Benthic iron and phosphorus fluxes across the Peruvian oxygen minimum zone. *Limnol. Oceanogr.* **57**(3), 851–867.

Nordli P. Ø., Hanssen-Bauer I. and Førland E.J. (1996) Homogeneity analyses of temperature and precipitation series from Svalbard and Jan Mayen. DNMI (Norwegian Meterol. Inst.) *Klima Rep*. No. **16/96**, 41.

Ohta Y., Hjelle A. and Dallmann W.K. (2007) Geological map Svalbard 1:100 000, sheet A4G, Vasahalvøya. Norsk Polarinstitutt Temakart No. **40**.

Ohta Y., Hjelle A. and Dallmann W. K. (2008) Geological map Svalbard 1:100 000, sheet A5G, Magdalenefjorden. *Norsk Polarinstitutt Temakart* No. **41**.

Ottesen D., Dowdeswell J. A., Benn D. I., Kristensen L., Christiansen H. H., Christensen O., Hansen L., Lebesbye E., Forwick M. and Vorren T. O. (2008) Submarine landforms characteristic of glacier surges in two Spitsbergen fjords. *Quat. Sci. Rev.* **27**(15–16), 1583–1599.

Pabi S., van Dijken G. L. and Arrigo K. R. (2008) Primary production in the Arctic Ocean, 1998–2006. *J. Geophys. Res.* **113**(C8), C08005. http://dx.doi.org/10.1029/2007JC004578.

Pakhomova S. V., Hall P. O. J., Kononets M. Y., Rozanov A. G., Tengberg A. and Vershinin A. V. (2007) Fluxes of iron and manganese across the sediment–water interface under various redox conditions. *Mar. Chem.* **107**, 319–331.

Perovich D. K., Richter-Menge J. A., Jones K. F. and Light B. (2008) Sunlight, water, and ice. Extreme Arctic sea ice melt during the summer of 2007. *Geophys. Res. Lett.* **35**, L11501. http://dx.doi.org/10.1029/2008GL034007.

Popova E. E., Yool A., Coward A. C., Aksenov Y. K., Alderson S. G., de Cuevas B. A. and Anderson T. R. (2010) Control of primary production in the Arctic by nutrients and light: insights from a high resolution ocean general circulation model. *Biogeosciences* **7**, 3569–3591.

Poulton S. W. and Raiswell R. (2002) The low-temperature geochemical cycle of iron: From continental fluxes to marine deposition. *Am. J. Sci.* **302**, 774–805.

Poulton S. W. and Canfield D. E. (2005) Development of a sequential extraction procedure for iron: implications for iron partitioning in continentally derived particulates. *Chem. Geol.* **214**, 209–221.

Poulton S. W. and Raiswell A. (2005) Chemical and physical characteristics of iron oxides in riverine and glacial meltwater sediments. *Chem. Geol.* **218**, 203–221.

Powell R. D. (1990) Glacimarine processes at grounding-line fans and their growth to ice-contact deltas. In *Glacimarine Environments: Processes and Sediments, Special Publication* No. **53** (eds. J. A. Dowdeswell and J. D. Scourse), Geological Society, London. pp. 53–73.

Premuzic E. T., Benkovitz C. M., Gaffney J. S. and Walsh J. J. (1982) The nature and distribution of organic matter in the surface sediments of world oceans and seas. *Org. Geochem.* **4**, 63–77.

Radić V. and Hock R. (2011) Regionally differentiated contribution of mountain glaciers and ice caps to future sea-level rise. *Nat. Geosci.* **4**, 91–94.

Raiswell R. (2006) Towards a global highly reactive iron cycle. *J. Geochem. Explor.* **88**, 436–439.

Raiswell R. and Canfield D. E. (1998) Source of iron for pyrite formation in marine sediments. *Am. J. Sci.* **298**, 219–245.

Raiswell R. and Anderson T. F. (2005) Reactive iron enrichment in sediments deposited beneath euxinic bottom waters: constraints on supply by shelf recycling. In *Mineral Deposits and Earth Evolution, Geological Society* (eds. I. McDonald, A. J. Boyce, I. B. Butler, R. J. Herrington and D. A. Polya). Geological Society of London Special Publication, London, pp. 179–194.

Raiswell R., Tranter M., Benning L. G., Siegert M., De'ath R., Huybrechts P. and Payne T. (2006) Contributions from glacially derived sediment to the global iron (oxyhydr)oxide cycle: implications for iron delivery to the oceans. *Geochim. Cosmochim. Acta* **70**, 2765–2780.

Raiswell R., Benning L. G., Tranter M. and Tulaczyk S. (2008a) Bioavailable iron in the Southern Ocean: the significance of the iceberg conveyor belt. *Geochem. Trans.* **9**, 10:1186/1467-4866-9-7.

Raiswell R., Benning L. G., Davidson L. and Tranter M. (2008b) Nanoparticulate iron minerals in icebergs and glaciers. *Mineral. Mag.* **72**, 345–348.

Raiswell R., Benning L. G., Davidson L., Tranter M. and Tulaczyk S. (2009) Schwertmannite in wet, acid, and oxic environments beneath polar and polythermal glaciers. *Geology* **37**, 431–434.

Raiswell R. and Canfield D. (2012) The iron biogeochemical cycle past and present. *Geochem. Perspec.* **1**(1), 220.

Reigstad M., Carroll J., Slagstad D., Ellingsen I. and Wassmann P. (2011) Intra-regional comparison of productivity, carbon flux and ecosystem composition within the northern Barents Sea. *Prog. Oceanogr.* **90**, 33–46.

Reimers C. E., Ruttenberg K. C., Canfield D. E., Christiansen M. B. and Martin J. B. (1996) Porewater pH and authigenic phases formed in the uppermost sediments of the Santa Barbara Basin. *Geochim. Cosmochim. Acta* **60**, 4037–4057.

Rich H. W. and Morel F. M. M. (1990) Availability of well-defined iron colloids to the marine diatom *Thalassiosira weissflogii*. *Limnol. Oceanogr.* **35**, 652–662.

Richard D., Sundby B. and Mucci A. (2013) Kinetics of manganese adsorption, desorption, and oxidation in coastal marine sediments. *Limnol. Oceanogr.* **58**(3), 987–996.

Rijkenberg M. J. A., Gerringa L. J. A., Timmermans K. R., Fischer A. C., Kroon K. J., Buma A. G. J., Wolterbeck B. T. and de Baar H. J. W. (2008) Enhancement of the reactive iron pool by marine diatoms. *Mar. Chem.* **109**, 29–44.

Rippin D., Willis I., Arnold N., Hodson A., Moore J., Kohler J. and Björnsson H. (2003) Changes in geometry and sublacial drainage of Midre Lovénbreen, Svalbard, determined from digital elevation models. *Earth Surf. Process. Landforms* **28**, 273–298.

Ronov A. B. (1982) The Earth's sedimentary shell (quantitative patterns of its structure, compositions, and evolution). *Intl. Geol. Rev.* **24**, 1313–1363.

Roy M., McManus J., Goñi M. A., Chase Z., Borgeld J. C., Wheatcroft R. A., Muratli J. M., Megowan M. R. and Mix A. (2013) Reactive iron and manganese distributions in seabed sediments near small mountainous rivers off Oregon and California (USA). *Cont. Shelf Res.* **54**, 67–79.

Rue E. L. and Bruland K. W. (1995) Complexation of iron(III) by natural organic ligands in the central north Pacific as determined by a new competitive ligand equilibration/absorptive cathodic stripping voltammetric method. *Mar. Chem.* **50**, 117–138.

Sakshaug E. (2004) Primary and secondary production in the Arctic Seas. In *The Organic Carbon Cycle in the Arctic Ocean* (eds. R. Stein and R. W. Macdonald). Springer-Verlag, Berlin Heidelberg, pp. 57–81.

Saloranta T. M. and Svendsen H. (2001) Across the Arctic front west of Spitsbergen: high-resolution CTD sections from 1998–2000. *Polar Res.* **20**(2), 177–184.

Sarmiento J. L. and Gruber N. (2006) *Ocean Biogeochemical Dynamics*. Princeton Univ Press, Princeton and Oxford, p. 503.

Schwertmann U., Stanjek H. and Becher H.-H. (2004) Long-term in vitro transformation of 2-line ferrihydrite to goethite/hematite at 4, 10, 15, and 25 °C. *Clay Miner.* **39**, 433–438.

Shaw T. J., Gieskes J. M. and Jahnke R. A. (1990) Early diagenesis in differing depositional environments: the response of transition metals in pore waters. *Geochim. Cosmochim. Acta* **54**, 1233–1246.

Shimada K., Kamoshida T., Itoh M., Nishino S., Carmack E., McLaughlin F., Zimmermann S. and Proshutinsky A. (2006) Pacific Ocean inflow: Influence on catastrophic reduction of sea ice cover in the Arctic Ocean. *Geophys. Res. Lett.* **33**, L08605. http://dx.doi.org/10.1029/2005GL025624.

Schoonen M. A. (2004) In *Mechanisms of sedimentary pyrite formation. In: Sulfur Biogeochemistry – Past and Present* (eds. J. P. Amend, K. J. Edwards and T. W. Lyons). p. 117–134.

Schubert C. J. and Calvert S. E. (2001) Nitrogen and carbon isotopic composition of marine and terrestrial organic matter in Arctic Ocean sediments: Implications for nutrient utilization and organic matter composition. *Deep Sea Res. Part I* **48**, 789–810.

Schulz H. D. (2006) Quantification of early diagensis: dissolved constituents in marine pore water. In *Marine Geochemistry* (eds. H. D. Schulz and M. Zabel). Springer, Heidelberg, pp. 75–124.

Seeberg-Elverfeldt J., Schlüter M., Feseker T. and Kölling M. (2005) Rhizon sampling of porewaters near the sediment-water interface of aquatic systems. *Limnol. Oceanogr.-Meth.* **3**, 361–371.

Severmann S., McManus J., Berelson W. M. and Hammond D. (2010) The continental shelf benthic iron flux and its isotope composition. *Geochim. Cosmochim. Acta* **74**, 3984–4004.

Sharp M., Parkes J., Cragg B., Fairchild I. J., Lamb H. and Tranter M. (1999) Widespread bacterial populations at glacier beds and their relationship to rock weathering and carbon cycling. *Geology* **27**, 107–110.

Shaked Y., Kustka A. B. and Morel F. M. M. (2005) A general kinetic model for iron acquisition by eukaryotic phytoplankton. *Limnol. Oceanogr.* **50**, 872–882.

Shaked Y. and Lis H. (2012) Disassembling iron availability to phytoplankton. *Front. Microbiol.* **3**, 123. http://dx.doi.org/10.3389/fmicb.2012.00123.

Shaw T. J., Raiswell R., Hexel C. R., Vu H. P., Moore W. S., Dudgeon R. and Smith, Jr., K. L. (2011) Input, composition, and potential impact of terrigenous material from free-drifting icebergs in the Wedell Sea. *Deep-Sea Res.* **58**, 1376–1383.

Siedlecki S. A., Mahadevan A. and Archer D. E. (2012) Mechansim for export of sediment-derived iron in an up-welling regime. *Geophys. Res. Lett.* **39**, L03601.

Skidmore M., Foght J. M. and Sharp M. J. (2000) Microbial life beneath a High Arctic glacier. *Appl. Envrion. Microbiol.* **66**, 3214–3220.

Skidmore M. L., Anderson S. P., Sharp M. J., Foght J. and Lanoil B. D. (2005) Comparison of microbial community compositions of two subglacial environments reveals a possible role for microbes in chemical weathering processes. *Appl. Envrion. Microbiol.* **71**, 6986–6997.

Skidmore M., Tranter M., Tulaczyk S. and Lanoil B. (2010) Hydrochemistry of ice stream beds-evaporitic or microbial effects? *Hydrol. Process.* **24**, 517–523.

Slagstad D., Ellingsen I. H. and Wassmann P. (2011) Evaluating primary and secondary production in an Arctic Ocean void of summer sea ice. An experimental simulation. *Prog. Oceanogr.* **90**, 117–131.

Ślubowska-Woldengen M., Rasmussen T. L., Koç N., Klitgaard-Kristensen D., Nilsen F. and Solheim A. (2007) Advection of Atlantic Water to the western and northern Svalbard shelf since 17,500 cal yr BP. *Quatern. Sci. Rev.* **26**, 463–478. http://dx.doi.org/10.1016/j.quascirev.2006.09.009.

Smith K. L., Robison B. H., Helly J. J., Kaufmann R. S., Ruhl H. A., Shaw T. J., Twining B. S. and Vernet M. (2007) Free-drifting icebergs: hot spots of chemical and biological enrichment in the Weddell Sea. *Science* **317**, 478–482.

Spencer K. L., Cundy A. B. and Croudace I. W. (2003) Heavy metal distribution and early-diagenesis in salt marsh sediments from Medway Estuary, Kent, UK. *Est. Coast. Shelf Sci.* **57**, 43–54.

Soetaert K., Hofmann A. F., Middelburg J. J., Meysmann F. J. R. and Greenwood J. (2007) The effect of biogeochemical processes on pH. *Mar. Chem.* **105**, 30–51.

Spielhagen R. F., Werner K., Sørensen S. A., Zamelczyk K., Kandiano E., Budeus G., Husum K., Marchitto T. M. and Hald M. (2011) Enhanced modern heat transfer to the Arctic by warm Atlantic water. *Science* **331**, 450–453.

Statham P. J., Skidmore M. and Tranter M. (2008) Inputs of glacially derived dissolved and colloidal iron to the coastal ocean and implications for primary productivity. *Global Biogeochem. Cy.* **22**, GB3013.

Stibal M., Šabacká M. and Žárský J. (2012) Biological processes on glaciers and ice sheet surfaces. *Nat. Geosci.* **5**, 771–774.

Sundby B. R., Anderson L. G., Hall P. O. J., Iverfeldt K., van der Loeff M. M. R. and Westerlund S. F. G. (1986) The effect of oxygen on release and uptake of cobalt, manganese, iron and phosphate at the sediment–water interface. *Geochim. Cosmochim. Acta* **50**, 1281–1288.

Sunda W. G., Barber R. T. and Huntsman S. A. (1981) Phytoplankton growth in nutrient rich seawater: importance of copper-manganese cellular interactions. *J. Mar. Res.* **39**(3), 567–586.

Svendsen H., Beszczynska-Møller A., Hagen J. O., Lefauconnier B., Tverberg V., Gerland S., Ørbæk J. B., Bischof K., Papucci C., Zajaczkowski M., Azzolini R., Bruland O., Wiencke C., Winther J.-G. and Dallmann W. (2002) The physical environment of Kongsfjorden-Krossfjorden, an Arctic fjord system in Svalbard. *Polar Res.* **21**, 133–166.

Syvitski J. P., Asprey K. W., Clattenburg D. A. and Hodge G. D. (1985) The prodelta environment of a fjord: suspended particle dynamics. *Sedimentology* **32**, 83–107.

Syvitski J. P. M., Burell C. D. and Skei J. M. (1987) *Fjords: Processes and Products*. Springer, New York.

Syvitski J. P. M. and Andrews J. T. (1994) Climate change: numerical modeling of sedimentation and coastal processes, eastern Canadian Arctic. *Arctic, Antarctic Alpine Res.* **26**, 199–212.

Syvitski J. P. M. and Lewis A. G. (1992) The Seasonal Distribution of Suspended Particles and Their Iron and Manganese Loading in a Glacial Runoff Fjord. *Geosci. Can.* **19**, 13–20.

Syvitski J. P. M. (2002) Sediment discharge variability in Arctic rivers: implications for a warmer future. *Polar Res.* **21**, 323–330.

Tagliabue A., Bopp L., Aumont O. and Arrigo K. R. (2009) Influence of light and temperature on the marine iron cycle: from theoretical to global modeling. *Global Biogeochem. Cy.* **23**, GB2017. http://dx.doi.org/10.1029/2008GB003214.

Taylor S. R. and McLennan S. M. (1985) *The Continental Crust: Its Composition and Evolution*. Blackwell, Oxford.

Taylor S. R. (1964) The abundance of elements in the continental crust: a new table. *Geochim. Cosmochim. Acta* **28**, 1278–1285.

Thuroczy C.-E., Gerringa L. J. A., Klunder M., Laan P., Le Guitton M. and De Baar H. J. W. (2011) Distinct trends in the speciation of iron between the shallow shelf seas and the deep basins of the Arctic Ocean. *J. Geophys. Res.* **116**, C10009.

Thuroczy C.-E., Alderkamp A.-C., Laan P., Gerringa L. J. A., Mills M. M., Van Dijken G. L., De Baar H. J. W. and Arrigo K. R. (2012) Key role of organic complexation of iron in sustaining phytoplankton blooms in the Pine Island and Amundsen Polynyas (Southern Ocean). *Deep-Sea. Res. Part II* **71–76**, 49–60.

Tovar-Sánchez A., Duarte C. M., Alonso J. C., Lacorte S., Tauler R. and Galbán-Malagón C. (2010) Impacts of metals and nutrients released from melting multiyear Arctic sea ice. *J. Geophys. Res.-Oceans* **115**, C07003. http://dx.doi.org/10.1029/2009JC005685.

Tranter M. (2005) Sediment and solute transport in glacial meltwater streams. In *Encyclopedia of Hydrological Sciences*, 169 (ed. M. G. Anderson). Wiley, New York, pp. 2633–2645.

Tranter M., Sharp M. J., Lamb H. R., Brown G. H., Hubbard B. P. and Willis I. C. (2003) Geochemical weathering at the bed of Haut Glacier d'Arolla, Switzerland-a new model. *Hydrol. Process.* **16**, 959–993.

Tranter M., Skidmore M. and Wadham J. (2005) Hydrological controls on microbial communities in subglacial environments. *Hydrol. Process.* **19**, 995–998.

Trusel L.D., Powell R.D., Cumpston R.M., and Brigham-Grette (2010) Modern glacimarine processes and potential future behaviour of Kronebreen and Kongsvegen polythermal tidewater glaciers, Kongsfjorden, Svalbard. In *Fjord systems and archives. Geological Society* (eds. J. A. Howe, W. E. N. Austin, M. Forwick and M. Paetzel). London, Special Publications, **344**, pp. 89–102, doi: 10.1144/SP344.9.

Van Cappellen P. and Wang Y. (1996) Cycling of iron and manganese in surface sediments: a general theory for the coupled transport and reaction of carbon, oxygen, nitrogen, sulfur, iron and manganese. *Am. J. Sci.* **296**, 197–243.

Van den Berg C. M. G. (1995) Evidence for organic complexation of iron in seawater. *Mar. Chem.* **50**, 139–157.

van der Merwe P., Lannuzel D., Bowie A. R. and Meiners K. M. (2011) High temporal resolution observations of spring fast ice melt and seawater iron enrichment in East Antarctica. *J. Geophys. Res.* **116**, G03017.

Vandieken V., Finke N. and Jørgensen B. B. (2006a) Pathways of carbon oxidation in an Arctic fjord sediment (Svalbard) and isolation of psychrophilic and psychrotolerant Fe(III)-reducing bacteria. *Mar. Ecol. Prog. Ser.* **322**, 29–41.

Vandieken V., Nickel M. and Jørgensen B. B. (2006b) Carbon mineralization in Arctic sediments northeast of Svalbard: Mn(IV) and Fe(III) reduction as principal anaerobic respiratory pathways. *Mar. Ecol. Prog. Ser.* **322**, 15–27.

Velle J. H. (2012) Holocene sedimentary environments in Smeerenburgfjorden, Spitsbergen. Master Thesis, University of Trømso.

Von Langen P. J., Johnson K. S., Coale K. H. and Elrod V. A. (1997) Oxidation kinetics of manganese (II) in seawater at nanomolar concentrations. *Geochim. Cosmochim. Acta* **61**(23), 4945–4954.

Wadham J. L., Cooper R. J., Tranter M. and Hodgkins R. (2001) Enhancement of glacial solute fluxes in the proglacial zone of a polythermal glacier. *J. Glaciol.* **47**, 378–386.

Wadham J. L., Bottrell S., Tranter M. and Raiswell R. (2004) Stable isotope evidence for microbial sulphate reduction at the bed of polythermal High Arctic glacier. *Earth Planet. Sci. Lett.* **219**, 341–355.

Wadham J. L., Cooper R. J., Tranter M. and Bottrell S. (2007) Evidence for widespread anoxia in the proglacial zone of an Arctic glacier. *Chem. Geol.* **243**, 1–15.

Wadham J. L., Tranter M., Skidmore M., Hodson A. J., Priscu J., Lyons W. B., Sharp M., Wynn P. and Jackson M. (2010) Biogeochemical weathering under ice: size matters. *Global Biogeochem. Cy.* **24**, GB3025.

Wadham J. L., Death R. M., Monteiro F. M., Tranter M., Ridgwell A. J., Raiswell R. and Tulaczyk S. (2013) The potential role of the Antarctic Ice Sheet in global biogeochemical cycles. *Earth Environ. Sci. Trans. R. Soc.* **104**(1), 55–67.

Wagner T. and Dupont L. (1999) Terrestrial organic matter in marine sediments: analytical approaches and eolian-marine records of the central Equatorial Atlantic. In *The Use of Proxies in Paleoceanography: Examples from the South Atlantic* (eds. G. Fischer and G. Wefer). Springer, New York, pp. 547–574.

Wang G., Spivack A. J., Rutherford S., Manor U. and D'Hondt S. (2008) Quantification of co-occurring reaction rates in deep subseafloor sediments. *Geochim. Cosmochim. Acta* **72**(14), 3479–3488.

Wells M. L., Mayer L. M. and Guillard R. R. L. (1991) A chemical method for estimating the availability of iron to phytoplankton in seawater. *Mar. Chem.* **33**, 23–40.

Weslawski J. M., Kendall M. A., Wlodarska-Kowalczuk M., Iken K., Kedra M., Legezynska J. and Sejr M. K. (2011) Climate change effects on Arctic fjord and coastal macrobenthic diversity-observations and predictions. *Mar. Biodiv.* **41**, 71–85.

Winkelmann D. and Knies J. (2005) Recent distribution and accumulation of organic carbon on the continental margin west off Spitsbergen. *Geochem. Geophys. Geosyt.* **6**(9), Q09012.

Yoshida T., Hayashi K. and Ohmoto H. (2002) Dissolution of iron hydroxides by marine bacterial siderophore. *Chem. Geol.* **184**, 1–9.

Yoshida M., Kuma K., Iwade S., Isoda Y., Takata H. and Yamada M. (2006) Effect of aging time on the availability of freshly precipitated ferric hydroxide to coastal marine diatoms. *Mar. Biol.* **149**, 379–392.

Zajączkowski J. and Legeżyńska J. (2001) Estimation of zooplankton mortality caused by an Arctic glacier outflow. *Oceanologia* **43**, 341–351.

Zajączkowski J., Bojanowski R. and Szczucinski W. (2004) Recent changes in sediment accumulation rates in Adventfjorden, Svalbard. *Oceanologia* **46**, 217–231.

Zajączkowski J. (2008) Sediment supply and fluxes in glacial and outwash fjords, Kongsfjorden and Adventfjorden, Svalbard. *Pol. Polar Res.* **29**(1), 59–72.

Ziaja W. (2001) Glacial recession in Sørkappland and central Nordenskiöldland, Spitsbergen, Svalbard, during the 20th century. *Arct. Antarct. Alp. Res.* **33**, 36–41.

Associate editor: Silke Severmann